Published in final edited form as:
Biochim Biophys Acta. 2013 ; 1827(0): 1278–1294. doi:10.1016/j.bbabio.2012.11.008.

Structural Analysis of Cytochrome bc_1 Complexes: Implications to the Mechanism of Function

Di Xia[1,¶], **Lothar Esser**[1], **Wai-Kwan Tang**[1], **Fei Zhou**[1], **Yihui Zhou**[1], **Linda Yu**[2], and **Chang-An Yu**[2]

[1]Laboratory of Cell Biology, Center for Cancer Research, National Cancer Institute, National Institutes of Health, Bethesda, MD 20892

[2]Department of Biochemistry and Molecular Biology, Oklahoma State University, Stillwater, Oklahoma 74078, USA

Summary

The cytochrome bc_1 complex (bc_1) is the mid-segment of the cellular respiratory chain of mitochondria and many aerobic prokaryotic organisms; it is also part of the photosynthetic apparatus of non-oxygenic purple bacteria. The bc_1 complex catalyzes the reaction of transferring electrons from the low potential substrate ubiquinol to high potential cytochrome *c*. Concomitantly, bc_1 translocates protons across the membrane, contributing to the proton-motive force essential for a variety of cellular activities such as ATP synthesis. Structural investigations of bc_1 have been exceedingly successful, yielding atomic resolution structures of bc_1 from various organisms and trapped in different reaction intermediates. These structures have confirmed and unified results of decades of experiments and have contributed to our understanding of the mechanism of bc_1 functions as well as its inactivation by respiratory inhibitors.

Keywords

cytochrome bc_1 complex; bifurcated electron flow; mechanism of ubiquinol oxidation; crystal structure; control of ISP domain movement

1. Functions of the cyt bc_1 complex

Ubiquinol cytochrome *c* oxidoreductase, commonly referred to as complex III or the cytochrome bc_1 complex (cyt bc_1 or bc_1), is a multifunctional, oligomeric membrane protein complex localized to the inner mitochondrial membrane of eukaryotes or the cytoplasmic membrane of prokaryotic organisms. This complex is an integral part of the cellular respiratory chain, contributing to the generation of electrochemical potential. Cyt bc_1 is also an essential part of the photosynthetic apparatus in purple bacteria, reducing cyt c_2 and returning it to the photosynthetic reaction center for oxidation. In plants, bc_1 complexes show integrated mitochondrial processing peptidase activity for cleavage of mitochondrial targeting signal peptides. Cyt bc_1 complexes have also been associated with the generation of reactive oxygen species (ROS). Alteration of bc_1 either by mutagenesis or by chemical treatment results in changes in function that often lead to devastating consequences.

[¶]Correspondence should be addressed to DX, xiad@mail.nih.gov, 37 Convent Dr., Building 37, Room 2122C, Bethesda, MD 20892.

1.1. Electron-transfer coupled proton-pumping function

The cyt bc_1 complex catalyzes the antimycin-sensitive electron transfer (ET) reaction from lipophilic substrate ubiquinol (QH_2) to cyt *c* coupled with proton translocation across the membrane [1]. As a result, for every QH_2 molecule oxidized, four protons are deposited to the positive side of the membrane and two molecules of cyt *c* are reduced. This stoichiometry of the ET reaction is given in the following equation, where QH_2 and Q represent lipid-soluble reduced and oxidized ubiquinone, respectively, c^{3+} and c^{2+} represent oxidized and reduced cyt *c*, and H^+_N and H^+_P represent protons at the negative and positive side of membrane. The cross-membrane potential thus generated serves as the energy source for various cellular activities such as the production of ATP by ATP synthase.

$$QH_2+2c^{3+}+2H^+_N \xrightarrow{bc_1} Q+2c^{2+}+4H^+_P$$

1.2. Mitochondrial processing peptidase activity

The cyt bc_1 complexes from higher organisms also exhibit mitochondrial processing peptidase (MPP) activity [2]. The MPP activity is readily detected in the purified bc_1 complex from plant mitochondria such as spinach; it is inactive (but can be activated with diluted detergents) in the bc_1 complex of bovine mitochondria [3]. The MPP activity occurs in the heterodimeric core-1 and core-2 subunits of the mitochondrial bc_1 (*Mtbc*$_1$), which belong to the pitrilysin family of zinc metallopeptidases, whose members include insulin-degrading enzyme and mitochondrial MPP in mammals and in fungi.

1.3. Superoxide generation

Under normal respiration conditions, the ET from QH_2 to cyt *c* catalyzed by the bc_1 complex is accompanied by the production of a small amount of superoxide anions presumably through electron leakage to molecular oxygen [4], which increases dramatically when the ET within the bc_1 complex is blocked by specific bc_1 inhibitors such as antimycin A or when the ET chain becomes over reduced. The most likely site of superoxide anion generation under normal ET conditions is at the site of low-potential cyt *b* heme (b_L heme). Mutations in the cyt *b* subunit result in not only impaired ET activity but also increased amounts of superoxide anions [5-7]. The role played by the small amount of superoxide anions generated under physiological conditions is not clear but has been speculated to be part of cellular signaling mechanisms [8].

2. Structural organization of cyt bc_1 complexes

Complex III was among the earliest discovered ET complexes in mitochondria. Cyt *b* was detected as early as in 1922 [9] and the first isolation procedure for complex III from bovine heart mitochondria was published in 1962 [10]. An estimated molecular mass of the complex was reported in 1965 [11]. It took another 32 years until the first crystal structure of bovine mitochondrial bc_1 (*Btbc*$_1$) was published in 1997 [12].

2.1. Subunit composition of bc_1 in various organisms

The subunit composition of bc_1 complexes varies significantly, from three subunits in *P. denitrificans* and *R. capsulatus* to as many as eleven subunits in human and bovine mitochondria (Table 1). All bc_1 complexes contain three redox subunits: cyt *b,* having two *b*-type hemes, a low potential heme b_L (E_{m7} = −90 mV for *bacterial* bc_1 and −30 mV for *Btbc*$_1$) and a high potential heme b_H (E_{m7} = +50 mV for bacterial bc_1 and +100 mM for *Btbc*$_1$); cyt c_1, containing a *c*-type heme (E_{m7} = +265 mV for bacterial bc_1 and +230 mV for *Btbc*$_1$); and the iron sulfur protein (ISP), including a high potential 2Fe-2S iron-sulfur

cluster (ISC, E_{m7} = +280 mV for bacterial bc_1 and +250 mV for $Btbc_1$). All additional subunits, referred to as supernumerary subunits, have no well-established cellular function except for the subunits core-1 and core-2 in plants, which are metalloproteases, and thus are believed to contribute to the increased stability of these complexes. Indeed, bc_1 complexes of eukaryotes carry more supernumerary subunits than those of prokaryotes, consistent with the fact that bc_1 complexes of higher organisms are generally more stable [13]. Furthermore, purified complex III contains ubiquinone and various phospholipids [14].

2.2. Structure determination - current status

Crystallographic studies of cyt bc_1 complexes have been approached in many different ways. There are currently 47 deposited experimental structures in the Protein Data Bank (PDB, Table 1). The first crystal structure obtained was for the ISP extrinsic domain (ISP-ED) fragment isolated by enzymatic treatment of bovine bc_1 [15, 16]. Remarkably, it was the bovine heart mitochondrial bc_1 containing no less than 11 different subunits and having a molecular weight of 490 *kDa* per dimer whose crystal structure was the first to be determined [12, 17, 18]. Structures of bc_1 complexes from yeast and non-oxygenic photosynthetic bacteria *R. sphaeroides and R. capsulatus w*ere later obtained (PDB IDs: 1EZV, 2QJP, and 1ZRT) [19-21]. More recently, the bc_1 structure from the soil bacterium *P. denitrificans* has also become available [22]. The high sequence similarity of bacterial bc_1 complexes to their mitochondrial counterparts makes them excellent model systems for mitochondrial enzymes. It should be mentioned that structures of related b_6f complexes from chloroplasts are also available [23], but an in-depth discussion of these works is outside the scope of this review. Because of the structural and functional complexities of the enzyme, all the structures determined by various research groups have provided information that revealed conformational intricacies of the complex and thus are not simply duplications of effort.

Structure determination of bc_1 in complex with various respiratory inhibitors has been particularly successful with mitochondrial bc_1 (Table 1), providing valuable insight into not only the mechanism of bc_1 function but also the mechanisms of inhibition by these inhibitors. Inhibitors such as stigmatellin play a critical role in stabilizing bc_1 in certain conformations suitable for crystal formation. For example, yeast bc_1 was crystallized in the presence of stigmatellin or HHDBT [19, 24]; bc_1 from *R. sphaeroides* can only be crystallized bound to certain types of inhibitors such as stigmatellin and famoxadone [25]. The functional significance of this conformational stabilization induced by inhibitor binding will be discussed later.

Cyt bc_1 complexes isolated from different organisms and with different protocols have been crystallized utilizing various procedures and have yielded different crystal forms. Purification and crystallization procedures can influence the subunit compositions of isolated complexes in solution or in crystalline state. While all eleven subunits of the bovine bc_1 have been observed [12, 17, 26, 27], the structures for yeast [19], chicken [18], and *R. sphaeroides* [21] each have one missing subunit. The structure of the mitochondrial bc_1 of *S. cerevisiae* was determined with a monoclonal Fv fragment bound to the ISP subunit, providing critical contacts for crystal formation [19].

2.3. Overall structure and subunit organization of bc_1

The crystal structures of mitochondrial bc_1 confirmed the results from electron crystallographic studies [28, 29] that the functional form of bc_1 is a dimer, as seen in all structures determined to date, and revealed the cross-talk of ISP subunits between symmetry-related monomers. They also confirmed the biochemically determined subunit composition [30] by showing that all eleven different subunits in bovine bc_1 are present in

crystals. Structures of the bc_1 complex can be divided into three regions: the membrane spanning, the inter-membrane space (periplasm in bacteria or positive side of the membrane), and the matrix (cytoplasm in bacteria or negative side of the membrane) regions (Fig. 1A). There are 13 transmembrane (TM) helices in a monomer of bovine mitochondrial bc_1; eight are contributed by the cyt *b* subunit and one each comes from cyt c_1, the ISP, subunits 7, 10, and 11. For bacterial bc_1 (Fig. 1B), the total number of TM helices is reduced to 10 or 11 for a monomer, depending on the presence or absence of the only supernumerary subunit. In mitochondrial bc_1, supernumerary subunits 1, 2, 6 and 9 are exclusively present in the matrix region. Notice, however, that the subunit 9 is absent in yeast bc_1 and none of these subunits are present in bacterial bc_1. Subunit 8 is associated with cyt c_1 at the intermembrane space side of the membrane for mitochondrial bc_1. Again, this subunit is absent in the bc_1 of bacteria.

From the first crystal structure of $Btbc_1$ [12], the positions of the iron atoms in prosthetic groups and distances between them were initially obtained by anomalous difference Fourier maps (Fig. 1C) and ET rates between pairs of prosthetic groups, serving as weakly coupled donors and receptors, can be estimated based on the empirical approximation for intraprotein ET transfer (Table 2) [31]. The permissible ET routes thus obtained were mostly consistent with proposed high and low potential chains. Surprisingly, the shortest distance between the iron-sulfur cluster (ISC) and the edge of c_1 heme is 27.7 Å, which corresponds to an estimated ET rate of 2.1×10^{-5} s^{-1}. This ET rate does not permit the normal function of bc_1. This conundrum was soon resolved, as it was discovered that the distance between the ISC and cyt c_1 is not a fixed parameter. Several refined crystal structures of bovine as well as chicken bc_1 revealed markedly different positions of the ISP-ED (Table 3), whereas the positions for *b* and c_1 hemes remained unchanged [17, 18].

2.4. Structures of the bc_1 subunits essential for ET function

Three subunits are essential for the ET function of bc_1: cyt *b*, cyt c_1 and ISP. In eukaryotes, cyt *b* is the only subunit encoded and synthesized by mitochondria; it is entirely embedded in the membrane and consists of two helical bundles: helices A-E form the first and helices F-H belong to the second. The two *b*-type hemes are intercalated into the first bundle between the TM helices B and D. As was correctly determined by genetic studies, the heme b_L was coordinated by the two histidine residues H83 and H182 (*Bt* cyt *b*) and the heme b_H was liganded also by two histidine residues H97 and H196. The two *b*-type hemes are part of the active sites that catalyze opposite reactions: the Q_P (Q_O near b_L heme) site, located near the inter-membrane space (IMS) in mitochondria or on the periplasmic side in bacteria, provides access to lipid-soluble QH_2 for oxidation, and the Q_N (Q_I near b_H heme) site, situated closer to the matrix (mitochondria) or cytoplasm (bacteria), carries out the reduction of ubiquinone. The two bundles contact each other on the negative side of the membrane, but separate on the positive side, creating a gap that is bridged by the cd helices (cd1 and cd2) and by the EF loop. A hydrophobic pocket below the cd helices and next to the ef helix is the ubiquinol oxidation site or Q_P pocket (Fig. 1D), which was first visualized by the binding of the Q_P specific inhibitor myxothiazol [12]. The location of the ubiquinone reduction site or the Q_N site was inferred from the antimycin-binding pocket of cyt *b* [12]. There are four prominent surface loops; three are on the positive side (AB, CD, and EF) and one is on the negative side (DE) (Fig. 1D).

Both the cyt c_1 and ISP subunits are anchored to the membrane by TM helices with their respective extramembrane domains localized on the positive side of the membrane (Fig. 1E and 1F). Whereas the TM helix of ISP is N-terminal to its extrinsic domain, the one for cyt c_1 is C-terminal. The extrinsic domain of the ISP subunit (ISP-ED) was found to be largely disordered in native and completely disordered in myxothiazol-bound bc_1 crystals of space

group $I4_122$ [12, 32], but was found ordered in different positions in crystals of space groups $P2_12_12_1$, $P2_1$, $P6_522$, and $P6_5$ [17, 18] (Table 3).

When sequences of *Mtbc*$_1$ and *Rsbc*$_1$ are compared, the latter often possess more insertions than deletions [21, 33]. Remarkably, the insertions occur only on or near the periplasmic or cytoplasmic side and not within the transmembrane region (Fig. 1B). An understanding of the functions of these additions or deletions may provide insight into the evolutionary process that transformed the bacterial enzyme into its mitochondrial equivalent. When compared to the bovine cyt *b*, the structure of bacterial cyt *b* is essentially identical. *Rs cyt b* features two terminal extensions and two major insertions. The N- and C-terminal extensions are 22 and 29 residues long, respectively; They each contains extramembrane helix named a0 and i, respectively (Fig. 1G). One insertion (de helix) is in the cytoplasmic DE loop and another (ef1 helix) is found after the ef helix on the periplasmic side. Thus, except for the ef1 helix, all extensions and insertions are located on the N-side of the membrane and they likely function to maintain the structural integrity of the quinone reduction site by preventing potential electron leakages and by safeguarding channels for proton influx. On the periplasmic side, there is one large insertion of 18 residues (310-327) between Pro^{285} and Asn^{286} (*Bt* cyt *b*) containing the ef1-helix, which protrudes from cyt *b* laterally and runs parallel to the membrane surface. This insertion occurs only in species that belong to the phylum proteobacteria. However, it is functionally important, as the point mutation S322A (*Rs* cyt *b*) or deletion of residues 309-326 (*Rs* cyt *b*) significantly lowers the enzyme activity [34]. The ef1-helix may play an important role in lipid binding, as features of several potential lipid molecules are visible in the electron density. It also enhances crystal contacts through aromatic stacking interaction between a pair of Trp^{313} residues from adjacent cyt *b* subunits [21].

Structure-based sequence alignment revealed that cyt c_1 of *Rsbc*$_1$ has undergone both insertions and deletions relative to mitochondrial complexes [21]. Apart from the two small insertions in the *Rs* cyt c_1 after Glu^{52} (4 residues) and Ala^{146} (3 residues), there is one large insertion between Gly^{109} and Gly^{127} (*Rs* cyt c_1). It features a short helix (H1d) that protrudes from cyt c_1 into the lipid bilayer sealing off a compartment between cyt c_1 and cyt *b* (Fig. 1H). The only insertion in cyt c_1 that may replace the function of a supernumerary subunit is the 18-residue insertion starting at position 162 (*Rs* cyt c_1), which is spatially close to the head domain of ISP. This region is characterized by an increased disorder (high B-factor) but features a stabilizing disulfide bridge (*Rs* cyt c_1, Cys^{145}-Cys^{169}), whose existence is in agreement with recently published data [35, 36]. Approximately 8 Å from the ISP-ED (Cα distance from cyt c_1 Asn^{173} to ISP Asp^{143}), this insertion presumably functions as an extended arm to limit its motion. Compared to mitochondrial cyt c_1, two large deletions, near residues Thr^{77} and Ser^{92} (*Rs* cyt c_1), respectively, result in the loss of bridging interactions between the two cyt c_1 subunits within the dimer.

Structure-based sequence alignment shows one insertion in the sequence of *Rs* ISP. This insertion (residues 97-108) is 20-25 Å from the *2Fe-2S* cluster and contributes to the surface of ISP-ED that faces away from cyt c_1; it forms a globular structure containing three β-turns and one inverse γ-turn (Fig. 1I). There is an intricate network of interactions employing both main chain and side chain atoms, suggesting a stabilizing role for this insertion. Disruption of this network of interactions by more than one point mutation led to the loss of the ISP subunit in the complex [37].

3. Mechanism of ET-coupled proton pumping from a structural perspective

3.1. Q-cycle and bifurcation of electron flow at the Q_P site

Unlike other ET complexes of the respiratory chain, the bc_1 complex uses ubiquinol to shuttle protons across the membrane and does so via the Q-cycle mechanism [38, 39] that obligates the bc_1 complex to have a quinol oxidation site, a quinone reduction site and a bifurcated ET at the quinol oxidation site (Fig. 2). The critical experiments that led to the Q-cycle hypothesis included oxidant-induced cyt *b* reduction in the presence of the bc_1 inhibitor antimycin [40, 41], identification of ISP as an oxidation factor [42], and the reaction stoichiometry of two protons translocated across the membrane for every electron transferred [43]. The identification of two postulated separate quinone reduction and quinol oxidation sites in the crystal structure further validated the "Q-cycle" mechanism [12].

The key step in the Q-cycle mechanism is the separation of the two electrons of the substrate QH_2 at the Q_P site. The first electron of quinol is transferred to the "high-potential chain", consisting of the ISP, cyt c_1 and cyt *c*. The second electron is concomitantly passed through the "low-potential chain" consisting of hemes b_L and b_H, to reduce ubiquinone or ubisemiquinone bound at the Q_N site. This mechanism ensures a proton pumping efficiency of two protons per electron transferred to cyt *c*.

Although the Q-cycle hypothesis has received much experimental support, it does not explain why the two electrons do not both follow the high potential chain, which is thermodynamically more favorable [44]. In fact, the chemistry underlying the electron bifurcation at the Q_P site has been hotly debated, resulting in many proposed mechanisms, including the catalytic switch model [45], the double-occupancy Qo site model [46], the proton-gated charge-transfer mechanism [47], the logic-gated fit mechanism [48], a sequential model [49, 50], a concerted model [51-53], more recently, the R-complex model [54], the double-gated model [55], and the proton-transfer gating mechanism [56]. A mechanism named "Surface-affinity modulated ISP motion switch hypothesis" was proposed on the basis of the observed conformational switch of the ISP in the analysis of crystallographic data in the presence of various bc_1 specific inhibitors [57, 58]. This and similar models [59] provides a simple explanation for the bifurcated ET at the Q_P site and its experimental basis will be outlined in the following sections.

3.2. Observed conformational change in the extrinsic domain of the ISP subunit in various crystal forms and in the presence of respiratory inhibitors

In the first $Btbc_1$ structure reported, the ISP-ED is at the *b*-position [12]. As shown in Table 2, the shortest edge-to-edge distance between the ISC and heme c_1 is 27.7 Å; ET along the high potential chain is not permissible under such conditions. Subsequent structure determinations showed ISP-ED in a number of different positions: near cyt c_1 (c_1-position) or at least two intermediate locations (*I*1- or *I*2-positions) (Table 3). When the ISP is at the c_1-position (*Bt* $P6_522$), the shortest edge-to-edge distance of cyt c_1 heme to atom ND2 of ^{Bt}H161 of the ISP, which is a ligand to the ISC, is measured at 7.8 Å, corresponding to an estimated ET rate of 2.9×10^7 s^{-1}. The two intermediate distances found in deposited PDB coordinates are *I*1-position of 23.6 Å (*Bt* $P6_5$) and *I*2-position of 14.9 Å (*Gg* $P2_12_12_1$). These distances would give ET rates of 0.007 s^{-1} and 1361 s^{-1}, respectively.

Crystallographic studies in the presence of various inhibitors have been conducted for $Btbc_1$, resulting in the observation of various conformations of the ISP-ED. Crystallographic studies of binding of Q_P site inhibitors to bovine bc_1 led to the classification of two types of inhibitors: P_f and P_m inhibitors [58]. The P_f inhibitors immobilize or fix the conformation of the ISP-ED at the *b*-position and include the classic inhibitors stigmatellin, n-undecyl

hydroxy dibenzothiazole (UHDBT), HDBT and n-nonyl quinoline N-oxide (NQNO), modern pesticides like famoxadone, 3-anilino-5-(2,4-difluorophenyl)-5-methyl-oxazolidine-2,4-dione (JG144), fenamidone and the natural inhibitor ascochlorin as well as iodo-crocacin-D (a compound optimized from natural crocacin D). P_m inhibitors release the ISP-ED from the *b*-position. This class of inhibitors contains the well-known natural inhibitor myxothiazol and also the synthetic compounds methoxy-acrylate stilbene and the widely used pesticides azoxystrobin, kresoxim methyl, trifloxystrobin, and triazolone.

Recently, structures of *Ggbc*$_1$ (chicken *bc*$_1$) in complex with either P_f or P_m inhibitors have been deposited into the Protein Data Bank (Table 1). In all P_f inhibitor complexes, the ISP-ED is found in the *b*-position, whereas in all P_m complexes, the ISP-ED is located in the *I2*-position. These structures are in complete agreement with what has been observed in inhibitor binding studies of *Btbc*$_1$ [12, 26, 32, 57, 58].

3.3. Domain movement is necessary but not sufficient for bifurcated electron flow

The crystallographically observed inherent mobility of the ISP-ED, as the ISP-ED was not well ordered in the first *bc*$_1$ structure [12] and the variable distances between the ISC and cyt c_1 heme in subsequent structures [17, 18] led to the proposal of ET by domain movement to bridge the 27.7 Å gap [17, 18]. Experimental attempts to immobilize the ISP-ED by mutations or by cross-linking in bacterial and yeast *bc*$_1$ complexes have invariably inactivated the enzyme [60-67], indicating that the mobility of the ISP-ED is necessary for the bifurcated ET of *bc*$_1$. However, whether the observed mobility of the ISP-ED is sufficient to guarantee an obligatory electron bifurcation is questionable. First, the observed rate (80,000 s^{-1}) of ET from the ISP to cyt c_1 in *Rsbc*$_1$ [68] is much faster than the turnover rate of the *bc*$_1$ complex (~900 s^{-1}), meaning that both electrons can potentially follow the high-potential chain. Second, the observed ET rate between the ISP and cyt c_1 is independent of pH and the redox potential of the ISP, indicating that the rate is not limited by the electron transfer event according to the Marcus theory. Instead, a gating or control mechanism for ISP-ED movement must be in place [69]. Third, addition of purified ISP-ED to a preparation of *bc*$_1$ without the ISP-ED only partially restores *bc*$_1$ activity [70]. Fourth, free motion of ISP cannot explain the total inhibition of *bc*$_1$ by antimycin, which acts remotely at the Q_N site. Thus, the mobility of ISP-ED itself is not sufficient to support a bifurcated ET at the Q_P site.

3.4. Capture and release of the ISP-ED is an inherent property of the cyt b subunit

The ISP subunits assemble into the *bc*$_1$ dimer with their respective N-terminal TM helices anchored in one monomer while their C-terminal ISP-EDs reach over to interact with the other monomer (Fig. 1A and 1B). A linker region (residues 62-74 in the *Bt* ISP), whose flexibility is essential for the electron-shuttling function of the ISP, provides the connection between the TM helix and the ISP-ED (Fig. 1F and 1I). The ISP-ED binds to the ISP-docking surface on the cyt *b* subunit through the small tip area that surrounds the *2Fe-2S* cluster and thus forms a part of the Q_P site. The tip of the ISP features a smooth, rigid, and largely hydrophobic surface suited to fit into a well-defined docking site.

Certain P_f inhibitors (stigmatellin and UHDBT) not only immobilize the ISP-ED but also increase its midpoint potential (E_{m7}). Both observations were explained by the formation of a direct H-bond between an oxygen atom of the inhibitor and the presumably protonated ^{Bt}H161 - a ligand of the *2Fe-2S* cluster. In particular, the formation of this H-bond had been deemed essential for the fixation of the ISP-ED at the *b*-position. Structural studies of a number of additional inhibitor-*bc*$_1$ complexes have appeared to support this notion [24, 54, 71]. However, this hypothesis is not compatible with the proposed Q_P site chemistry for ubiquinol oxidation, which involves the formation of a hydrogen bond

between the substrate ubiquinol and the ISP, because ubiquinol cannot act as an inhibitor. Surprisingly, the bc_1-famoxadone and bc_1-JG144 complexes showed the ISP-ED in the fixed state as observed in the stigmatellin complex, yet there was no direct ISP-inhibitor interaction (Fig. 3A and 3B). It is therefore clear that direct H-bonding between the ISP-ED and the bound inhibitor may contribute to, but does not cause the conformational fixation of the ISP. Instead, the conformational switch of the ISP is an intrinsic property of the bc_1 complex.

If the conformational switch or capture-and-release of the ISP-ED is indeed an intrinsic property of bc_1, an important question is whether the ISP-ED can undergo the fixed to mobile conformational transition in the absence of inhibitor binding, as this is highly relevant to bc_1 function under physiological conditions. Preliminary results from redox-coupled crystallographic studies of $Btbc_1$ [72, 73] showed ISP-ED is in the fixed position when the complex is fully reduced, whereas it is mobile when oxidized. Thus, conformation transition of the ISP-ED can also be achieved with electronic signals, most likely from ET in the cyt *b* subunit.

3.5. Mechanism of ISP-ED's capture and release

The ISP binding surface of cyt *b* has the appearance of a volcanic crater; most residues that contribute to the crater are hydrophobic in nature and only 16 of them have side chains facing the ISP. Of these residues, all but one are located on the CD and EF loops, which connect helices C and D, and helices E and F, respectively (Fig. 1D and 1G). Two structural motifs within the CD and EF loops, the conserved cd1 helix and the PEWY sequence motif, undergo large movements upon binding of Q_P site inhibitors. Inhibitor binding generally causes the PEWY motif, as measured for residue ^{Bt}P271 of bovine cyt *b*, to back away in a unidirectional fashion from the Q_P pocket by more than 1.5 Å, whereas the direction in which the cd1 helix moves clearly correlates with the type of bound inhibitors when compared to the structure of inhibitor-free bc_1. Invariably, the inhibitors that are known to promote the mobile state of the ISP-ED cause a negative shift, whereas all inhibitors that cause the capture of the ISP at the Q_P site lead to a positive displacement of the cd1 helix; here the positive or negative denotes the direction of the shift relative to the inhibitor-free enzyme. More precisely, the positional shifts of the cd1 helix are roughly parallel to the membrane surface; the positive shift signifies a displacement of the cd1 helix swinging outward away from the Q_P pocket leading to an expanded Q_P pocket, and the negative shift indicates an inward displacement. The importance of the cd1 helix in bc_1 function is also manifest in its high degree of sequence conservation, which reaches 98.5% identity (averaged over 14 residues), based on an analysis of a 5,355 non-redundant cyt *b* sequence set, as compared to the cd2 helix (73.5% for 9 residues) or to the whole subunit (75.2% for 379 residues), a fact that has been known for a long time but had no clear explanation [74].

The mechanism that induces this dramatic transition in ISP-ED conformation and how the signal is transmitted from the source (the binding of inhibitor to the Q_P site) to the target residue(s) that capture the ISP-ED have been investigated [57]. Two possible interaction forces at the ISP-ED binding surface were looked at separately without assuming that they were mutually exclusive: (1) changes in hydrogen bonding patterns and (2) adjustments in van der Waals (vdw) interactions expressed as changes of surface complementarity. It is conceivable that, if the bifurcation of ET requires a control mechanism for ISP-ED conformational switch, the formation of a large number of strong H-bonds between the docked ISP-ED and the docking site would be unfavorable for the switch for energetic reasons. Indeed, in the structures where the ISP-ED is in the fixed conformation or *b*-position as seen in the complexes of P_f inhibitor famoxadone, stigmatellin, JG144, NQNO, UHDBT, ascochlorin or crocacin as few as seven H-bonds are formed between the ISP and cyt *b*. While two of them are permanent and found in the neck region of the ISP of all

structures, the remaining five H-bonds are made with the ISP-ED as long as the ISP remains docked. Most notably, only carbonyl oxygen atoms of the backbone are employed by the ISP for non-permanent H-bonds. The non-permanent H-bonds disappear when P_m inhibitors like azoxystrobin, MOA-stilbene or myxothiazol are bound. Extensive mutagenesis studies in the cyt b subunit including the ^{Rs}K287-S151 dyad and ^{Sc}Y278 (^{Rc}Y302) [7, 57] appear to rule out that the change in H-bonding pattern controls ISP capture and release.

When the van der Waals interactions were examined (expressed in terms of changes in contact area (CA) and in surface complementarity (SC) of the two interacting surfaces between the cyt *b* and the ISP-ED), it was clear that changes in CA and SC are correlated to the movement of the cd1 helix. As one goes from P_f- to P_m-type inhibitors, there is a decrease in the CA and most notably a nearly 40% loss in SC. Since the ISP-ED has shown no sign of internal plasticity and the cd1 helix is known to undergo a shear motion as inhibitors bind to the Q_P site, the change in shape complementarity caused by the cd1 motion represents a possible mechanism that could account for the change in binding affinity of cyt *b* toward the ISP, thus regulating ISP conformational dynamics.

Although the cause and effect relationship is apparent for the binding of different types of inhibitors and the conformational switch of the ISP-ED, the same relationship cannot be said with absolute certainty for the movement of the cd1 helix and the ISP-ED switch. However, circumstantial evidence does exist. (1) Inhibitors such as famoxadone do not contact the ISP-ED directly. Thus capture of the ISP-ED by famoxadone binding likely follows the sequence of inhibitor binding to cyt *b*, followed by cd1 helix movement, changing the shape of the ISP-ED binding crater, and subsequent ISP-ED arrest. (2) ISP-ED conformational switch can be mediated by changes in redox conditions in the absence of inhibitors. Under such conditions, the reduction of cyt *b* likely signals the movement of the cd1 helix, leading to capture of the ISP-ED. (3) Even before the role of the cd1 helix was proposed, the activity of bc_1 was found to be dependent on the size of the residue at position 155 of the cd1 helix (*Rsbc*$_1$). The larger the size of the side chain, the less activity the bc_1 complex has [75]. Examination of bc_1 structure indicates that mutation of residue ^{Rs}S155 to a larger residue would limit the movement of the cd1 helix, leading to inactivation.

3.6. Affinity controlled ISP conformational switch hypothesis for bifurcated ET at Q_P site

A control mechanism, called the “binding affinity modulated ISP-ED motion switch hypothesis” has been proposed, allowing modulation of the binding affinity toward the ISP-ED by the cyt *b* subunit [57, 76] (Fig. 4). The basic principle of the hypothesis is that the cyt *b* subunit controls the rate of electron flow in the high potential chain by controlling the ISP-ED conformation state and regulating the distance between the ISC and heme c_1, thus ensuring the bifurcated flow of the two electrons from ubiquinol. The following sequence of events during the QH_2 oxidation may take place: (1) In the absence of any substrate at the Q_P site, the ISP-ED is capable of sampling the Q_P site frequently. The binding surface on the side of cyt *b* is in a resting state in a sense that its shape matches that of the ISP-ED sufficiently well to keep it in proximity but not enough to hold it in a fixed conformation. This state is characterized by the ef helix in the “closed” position and the cd1 helix in the “resting” position. (2) When a substrate QH_2 molecule enters the catalytic site (Fig. 4, step 1), it proceeds to the distal part of the Q_P pocket. To accommodate the QH_2 molecule, the ISP-binding crater widens by moving the cd1 switch toward the “on” position and by pushing the ef helix to the “open” position. The reshaping of the ISP-binding site increases its affinity for the ISP-ED to the point of its fixation *in situ*. As a result, a transient cyt *b*-QH_2-ISP complex forms, which features an H-bond from ^{Bt}H161 of the ISP to the substrate. The distance from the ISC to heme c_1 is now fixed at 27.7 Å. (3) As the first electron is being transferred to the ISP (Fig. 4, step 2), the one-electron carrier remains fixed in place, and the second electron in the Q radical has to enter the low-potential chain, a process that

likely occurs simultaneously with the first ET and possibly via residue ^{Bt}Y131, which undergoes a large conformational change when bound with UHDBT [58]. The notion of a concerted ET is supported by the inability to detect an ubisemiquinone radical on the EPR time scale and by the observation of simultaneous reduction of the ISP and b_L heme in pre-steady-state kinetic analysis of the ET at the Q_P site [52]. We speculate that as the second electron moves toward the b_H heme (Fig. 4, step 3), the proton translocation is accomplished. It is worthwhile to emphasize that because the reduced ISP is fixed at the *b*-position, which is at a non-permissive distance from c_1 heme for ET, the first electron remains in the ISP. This simple mechanism ensures the bifurcated ET of the two electrons. (4) The Q molecule exits via the proximal binding site in the Q_P pocket; this event would reverse the pressure on the cd1 helix, retract it to the "off" position, and cause the release of the ISP-ED. The ef helix stays at the open position until the product exits the Q_P pocket (Fig. 4, step 4).

An important concept of this hypothesis is that the ISP-ED remains fixed at the Q_P site or *b*-position until the transfers of the second electron and protons from ubiquinol are completed, which effortlessly explains the high fidelity of the bifurcation of the electron pathway. This hypothesis is consistent not only with structural data but also with a great deal of biochemical, biophysical and genetic evidence: (1) it provides a functional explanation for the extraordinary sequence conservation of the cd1 helix. (2) A logical consequence of this hypothesis is that the reduction of *b* hemes precedes that of cyt c_1, as shown by the pre-steady state kinetic analysis [52, 77-79]. (3) It agrees well with the observations that mutations introduced into the ISP-ED binding surface mostly affect the ET kinetics between the ISP and cyt c_1 but rarely influence the substrate binding, as in ^{Rs}K329A of *R. sphaeroides* [57], ^{Sc}W142 of yeast [80], ^{Rs}L286 and ^{Rs}I292 of *R. sphaeroides* [81], ^{Rs}K329 of *R. sphaeroides* [82], ^{Sc}Y279 of yeast (^{Rc}Y302 in *R. capsulatus*) [6, 7] and ^{Rs}T160 of *R. sphaeroides* [83]. (4) The hypothesis predicts that limiting the movement of the cd1 helix leads to modification in the activity of the complex depending on the size of substitution, as seen in ^{Rs}S155 of *R. sphaeroides* [75] and in ^{Rc}G158 of *R. capsulatus* [84]. (5) Since antimycin is known to act remotely at the Q_N site, it would be difficult to explain how antimycin could completely inhibit steady state bc_1 activity, especially in the context of ISP head domain undergoing a free motion. The observed redox-dependency of ISP-ED conformational switch shows an immobilized ISP-ED when bc_1 is fully reduced, which readily explains the strict inhibition of bc_1 by antimycin.

Despite its simplicity as a control mechanism for bifurcation of electron flow at the Q_P site, this hypothesis does not adequately define the signaling pathway that triggers the capture and release of ISP-ED under physiological conditions. One possibility is that the ET from hemes b_L to b_H causes protein conformational changes in the cd1 helix and allows or forces the reduced ISP-ED to move from the *b*-position to the c_1-position to be oxidized [85, 86]. Such a redox-induced conformational change in the cyt *b* subunit has yet to gain direct experimental support. A second possibility involves the binding of the substrate QH_2 to and exit of the reaction product Q from the Q_P site, leading to capture and release of the ISP-ED [32].

4. Interaction with substrates, lipids, inhibitors and metal ions

4.1. Interaction with cytochrome c

Despite the presumed transient interaction between bc_1 and cyt *c*, the crystal structures of bc_1 in complex with either isoform-1 or -2 of cyt *c* of *S. cerevisiae* were obtained to 2.97 Å resolution for the oxidized cyt *c* and to 1.9 Å resolution for the reduced cyt *c*, respectively [87, 88]. It should be mentioned that in both cases the complex was crystallized in the presence of a bound Fv fragment derived from a monoclonal antibody and Q_P site inhibitor

stigmatellin. As expected, the cyt *c* binds to the c_1 subunit of bc_1. Surprisingly, however, the binding is sub-stoichiometric with one cyt *c* bound to one c_1 subunit, while the second site on the bc_1 dimer remains unoccupied or possibly exhibits very low occupancy or severe disorder. The binding forces were characterized as mostly nonpolar in nature. The close spatial arrangement of the two cytochromes reduces the distance between the CBC atoms of the two respective heme vinyl groups to 4.5 Å and the distance between the two iron centers to 17.4 Å. Furthermore, the observed interplanar angle of the heme groups is 55°, suggesting a direct and rapid heme-to-heme electron transfer at a calculated rate of up to $8.3 \times 10^6\ s^{-1}$. In the structure, no direct interaction has been observed between subunit QCR6 and cyt *c*; the former is a small acidic protein thought to be involved in cyt *c* binding.

In the reduced state, the dimer structure is asymmetric, as the binding of monovalent cyt *c* is correlated with conformational changes in the ISP-ED and subunit QCR6 and with a higher number of interfacial water molecules bound to cyt c_1. There exists a mobility mismatch at the interface, with disordered charged residues on the cyt *c* side and ordered ones on the cyt c_1 side, which could be significant for transient interactions [88].

4.2. Interaction with ubiquinone at the Q_N site

Assignments of bound substrate ubiquinone (Q) have only been made to the Q_N site. Initial indication for bound Q came from the difference density map between antimycin–bound and native crystals [12], as a negative density appeared in a pocket in the TM region of cyt *b* next to the b_H heme site, which represented part of a ubiquinone molecule that is bound in the native crystal but is displaced by bound antimycin A. This suggests that the antimycin binding site partly overlaps the quinone reduction site Q_N. In the yeast structure [19], a Q6 (ubiquinone with six isoprenoid repeats) was fitted into the electron density in the Q_N site. In bovine and *R. sphaeroides* bc_1, a Q2 was identified [21, 27, 58].

As no ubiquinone was added, the natural substrate identified in the native bc_1 crystal (1NTZ, Table 1) was obviously retained during purification and crystallization. In the refined bovine bc_1 structure [27], a piece of electron density was located at the Q_N site of the cyt *b* subunit more than 5σ above the mean, into which a ubiquinone molecule with its first two isoprenoid repeats was fitted. The two possible orientations of the planar ubiquinone ring could not be distinguished from the shape of the electron density (Fig. 3C). The average *B* factor of the bound ubiquinone is twice as large as its immediate protein environment, suggesting most likely a lower than 50% occupancy in the crystal. The quinone ring is nearly perpendicular to the plane of the phenyl ring of ^{Bt}F220 and to that of heme b_H; the former forms an Ar-Ar pair with the ubiquinone (3.0 Å), and the latter has the closest distance of 4.2 Å. There are three H-bonds formed between the bound ubiquinone and the Q_N site residues ^{Bt}D228, ^{Bt}H201 and ^{Bt}S205; some of these H-bonds are mediated by water molecules. The two isoprenoid repeats that were visible in the electron density are in contact with residues ^{Bt}P18, ^{Bt}S35, ^{Bt}G38, ^{Bt}M190, ^{Bt}L197, and the b_H heme. The van der Waals surface of the matrix side of these TM helices, particularly in cyt *b*, features channels leading to the Q_N site and serving as possible proton uptake pathways. Conformational changes in residues contacting bound quinone, as exhibited in crystal structures of yeast and bovine bc_1, implicate possible mechanisms for proton uptake from the matrix into the Q_N pocket [27].

In the $Rsbc_1$ structure the natural substrate Q bound to the crystalline bc_1 is estimated to have 70% occupancy based on the comparison of average B factor of the Q to side chain atoms of surrounding, interacting residues [21]. The quinone molecules are roughly perpendicular to the parallel planes of ^{Rs}F216 and heme b_H on one side and parallel to the plane of ^{Rs}F244 on the other side. When the six monomeric bc_1 structures from a crystallographic asymmetric unit are aligned, the positions and orientations of bound Q are

different; the largest positional and rotational displacements are 1.3 Å and 38°, respectively. Residue ^{Rs}H217 (^{Bt}H201) forms H-bonds with Q molecules with the O2-NE2 distances in the range of 2.2–2.4 Å, indicating that the imidazole ring of ^{Rs}H217 follows the motion of Q, consistent with its observed conformational flexibility.

4.3. Interaction with bound lipid and detergent molecules

Cyt bc_1 is an integral part of the cellular membrane and consequently, lipid molecules play an essential role in its function [89, 90]. In eukaryotic cells, a characteristic phospholipid is cardiolipin, which primarily exists in mitochondria and was shown to be essential for the function of bc_1 [14]. Crystal structures of bc_1 from various species have revealed bound lipid molecules [21, 91]. The roles of these bound lipid molecules are proposed to be two fold: promoting structural integrity of the complex and stimulating enzyme activity. Structural assignment and functional analysis for five crystallographically resolved bound lipid molecules was described for yeast bc_1 [91]: two phosphatidylethanolamines (PE), one phosphatidylcholine (PC), one phosphatidyinositol (PI), and one cardiolipin (CL) and one detergent molecule DDM. These molecules are bound to the TM region at the surface of the two monomers and in two large lipophilic clefts that are present at the dimer interface. Their head groups are bound to the protein surface in regions with positive electrostatic potential. The assignments were solely based on the appearance of electron density.

Two lipid molecules have been described in considerable detail in the yeast complex: a PI molecule was found to bind in an unusual interhelical position near the flexible linker region of the ISP and a CL is positioned at the entrance of a proposed proton uptake site. The mutagenesis analysis of the CL site showed that CL binding is critical for the respiratory super complex formation [92].

In crystals of *Rsbc*$_1$, ordered lipid molecules are often found on the boundary surface between symmetry-related dimers, at the dimer or subunit interfaces, and in surface depressions [21]. One lipid molecule was positively identified on the N-side of the membrane and included in the model. However, additional lipids that are only partially recognizable at both sides of the membrane were excluded in final models. The lipid molecule bound at the cytoplasmic surface of cyt *b* is modeled as a lauryl oleoyl phosphatidyl ethanolamine (PE); its head group aligns with the surface plane of the cytoplasmic leaflet of the membrane and its fatty acid chains flank the TM helices B and G of cyt *b* (Fig. 3D). The exact identities of the fatty acids are unknown but the assignment as PE is supported by comparing it to the lipids present in bovine and yeast bc_1. The phosphate group is hydrogen bonded to two highly conserved consecutive tyrosine residues (^{Rs}Y117 and ^{Rs}Y118), and the lipid head group is further stabilized by the side chain of ^{Rs}R358 by forming an ion pair with the lipid phosphate.

At the N-terminal end of the ef1 insertion in cyt *b*, which is unique to bc_1 of bacteria, the side chain of ^{Rs}W313 forms a stacked pair with its symmetry-mate from a neighboring dimer at a distance of 3.8 Å. This pair is symmetrically flanked by at least six pieces of extra electron density, most likely stemming from bound lipid or detergent molecules [21]. A strontium ion, clearly confirmed by its anomalous signal, sits right above the indole rings of the tryptophan pair. Its exact coordination environment cannot be resolved, but might involve the head groups of two pairs of putative lipid molecules. We observed the tryptophan pair formation in all crystal forms, and the presence of strontium ions seems to strengthen the interaction but is not required.

4.4. Interaction with Q_N and Q_P site inhibitors

As a central component of the cellular respiratory chain, the bc_1 complex became an easy target for numerous natural antibiotics, as a result of constant battle for survival over the course of evolution. Examples of natural compounds that specifically target the bc_1 complex are antimycin A, strobilurin, myxothiazol, and stigmatellin. Many of the earlier functional and mechanistic studies of the bc_1 complex were facilitated by the use of these inhibitors, which block ET at selected points [93]. Structural analysis of bc_1 complexes also benefited from these inhibitors, as they stabilize certain conformations at a given state. By manipulating differences in uptake between the host and pathogens, some of the inhibitors or their derivatives have been developed into anti-fungal and anti-parasitic agents and are used in agriculture to control fungal or bacterial diseases and in medicine to treat infections.

Historically, bc_1 inhibitors were classified based on their effects on b_L-heme spectrum and impact on the redox potential of the ISP, due to a lack of understanding of the underlying process [94]. On the basis of structural information, bc_1 inhibitors are currently divided into Q_P site inhibitors (P), the Q_N site inhibitors (N) and the dual site inhibitors (PN) [58]. An increasing body of structural evidence starting with the first structures of bc_1 [12] followed by a number of high resolution inhibitor bound bc_1 complex structures suggested that the influence of the inhibitor on the mobility of the ISP-ED was systematic. Accordingly, all known Q_P site inhibitors can be divided into two subgroups [57, 58], namely those that fix the conformation of the ISP-ED in the *b*-position (P_f-type) and those that mobilize it (P_m-type). In the latter case, the ISP-ED may be found in the c_1-position (PDB IDs: 3L70, 3L71, and 3L72) but could also be anywhere between the *b* and c_1-position (PDB IDs: 1SQP and 1SQQ).

The class of known P_f inhibitors encompasses stigmatellin, UHDBT, HDBT, NQNO**,** famoxadone, JG144, fenamidone, ascochlorin and iodo-crocacin-D. The class of P_m inhibitors contains the well-known natural inhibitor myxothiazol but also the synthetic compounds methoxy-acrylate stilbene and the widely used pesticides azoxystrobin, kresoxim methyl**,** trifloxystrobin, and triazolone**.** This group contains derivatives of strobilurin, whose structure-activity relationship advanced the research in respiratory chain complex III inhibitors. Given the consistency of the mode of binding in this group, it could be expected that all methoxy-acrylates, methoxy-carbamates, oximino-acetates, oximino-acetamides and benzyl-carbamates would belong to this group. The class of N inhibitors is comprised of compounds that occupy the Q_N site. This group is still rather small and starts with the natural inhibitor antimycin but also contains NQNO and ascochlorin**,** for which crystal structures were determined (Table 1). No structural information is currently available that would illuminate how a number of natural inhibitors like funiculosin or the important pesticides cyano-imidazole (cyazofamid**)** and sulfamoyl-triazole (amisulbrom) might bind. The class of PN inhibitors is essentially not a new class, as members of this group are listed in both the P and N class (Table 1). Its presence only underlines the fact that some inhibitors have features (just as the quinol/quinone pair) that allow them to bind to both active sites. This group includes NQNO, ascochlorin and tridecyl-stigmatellin (observed in b_6f) [95].

4.5. Interaction with metal ions

When incubated with mother liquor containing 200 μM $ZnCl_2$ for seven days, the crystalline chicken bc_1 complex specifically binds Zn^{2+} ions at two identical sites or one per monomer in the dimer [96]. Zinc binding occurs close to the Q_P site and is likely to be the reason for the inhibitory effect on the activity of bc_1 observable during zinc titration [97, 98]. The Zn^{2+} ion binds to a hydrophilic area between cytochromes *b* and c_1 (PDB: 3H1K) and is coordinated by ^{Gg}H212 of cyt c_1, ^{Gg}H268, ^{Gg}D253, and ^{Gg}E255 of cyt *b*, and might interfere with the egress of protons from the Q_P site to the intermembrane aqueous medium.

No Zn^{2+} was bound at the zinc binding motif of the putative MPP active site of core-1 and core-2 for chicken bc_1 after prolonged soaking [96] nor was it found in the native bovine or yeast structures [12, 19].

Crystals of $Rsbc_1$ grown in the presence of strontium ions revealed several Sr^{2+} binding sites. One site that is not present in mitochondrial bc_1 but appears to be conserved in photosynthetic bacteria is on cyt c_1 [21]. The strontium ion, confirmed by the appearance of a strong anomalous signal from the data set collected above the strontium absorption edge, is accessible from the periplasm and coordinated by side chains of ^{Rs}D8, ^{Rs}E14, and ^{Rs}E129 as well as by the backbone carbonyl oxygen atom of residue ^{Rs}V9 in a distorted octahedron. At the N-terminal end of the ef1 insertion in cyt *b*, the side chain of ^{Rs}W313 forms a stacked pair with its symmetry-mate from a neighboring dimer at a distance of 3.8 Å. A strontium ion, clearly confirmed by its anomalous signal, sits right above the indole rings of the tryptophan pair. In this case the role of strontium ions seems to reinforce the interaction of the tryptophan pair.

5. Structures of supernumerary subunits and their functional implications

Common to all bc_1 complexes are the three subunits that contain redox prosthetic groups. In higher organisms, there are additional subunits with more than half of the total molecular mass of the complex, which are called supernumerary subunits. The role of these subunits has been a matter of debate. Since they are not required for the ET function of bc_1, it was previously assumed that the additional subunits had structural rather than functional roles. The supernumerary subunits include two large extrinsic proteins named core-1 and core-2, and another four to six smaller subunits of molecular mass under 15 *kDa*. Most supernumerary subunits are not embedded in the membrane, but peripherally localized at the membrane surfaces, mostly at the matrix side of the membrane.

5.1. Structures of core-1 and core-2 subunits of mitochondrial bc_1

The core proteins contribute to more than one-third of the total mass of the bc_1 complex. The function of the core proteins in non-plant species is not understood fully. They are, however, required for full activity and stability of the bc_1 complex [99]. In yeast, the core proteins were shown to be required for assembly of the complex [100]. In plants, the core proteins have a unique peptidase function [2, 101].

The core-1 and core-2 subunits of bovine bc_1 are synthesized in the cytosol as precursor proteins of 480 and 453 amino acid residues, respectively, which are proteolytically processed as they are being transported into mitochondria by removing 34 and 14 residues, respectively, from the N-termini of core-1 and core-2 precursors. Core-1 and core-2 share 21% sequence identity and expectedly, their three-dimensional structures are remarkably similar (Fig. 5A and 5B). Each of the core subunits consists of two structural domains of about equal size and almost identical folding topology, which are also related by approximately two-fold rotation symmetry, even though only about 10% of the residues are chemically identical. Both domains are folded into one mixed β-sheet of five or six β-strands, flanked by three α-helices on one side and one α-helix from the other domain on the other side.

The overall shape of each core protein resembles a bowl. In the assembled $Btbc_1$ complex, the N-terminal domain of core-1 interacts with the C-terminal domain of core-2, and vice versa (Fig. 5C). Core-1 and core-2 enclose a large, acidic cavity that was also observed by electron microscopy [29] (Fig. 5D). Because the two internal approximate two-fold rotation axes of core-1 and core-2 differ in direction by 14.5°, the two bowls representing these proteins come together in the form of a ball with a crevice leading to the internal cavity (Fig.

5D). The crevice is filled with peptide fragments that were assigned as part of subunit 9, a signal peptide of the ISP subunit [12]. The amino acid residues lining the wall of the cavity are mostly hydrophilic.

Yeast COR1 and QCR2 have sequence homologies of 51% and 50% to the corresponding core-1 and core-2 subunits of bovine bc_1, respectively [19]. The differences between the two species are most pronounced in the C-terminal domain of QCR2. The subunit is 68 residues shorter than the corresponding bovine core-2; its N-terminal domain has a five-stranded β sheet, whereas the bovine core-2 is six-stranded. In the bovine complex the cleaved signal peptide of the ISP (subunit 9) is located in the crevice between the core-1 and core-2 proteins [12], the binding of which is stabilized by hydrophobic interactions with this β sheet. Polar or charged residues are present at the corresponding positions in yeast [19]. Thus, this cavity formed between COR1 and QCR2 is larger in yeast and open to the bulk solvent and no electron density was found for a retained signal peptide.

The core-1 and core-2 heterodimer of $Mtbc_1$ is thought to be a relic of the broad family of metalloproteases. In particular, the core proteins of mammalian bc_1 complexes are homologous to the subunits of the general mitochondrial matrix processing peptidase (MPP), which cleaves signal peptides of nucleus-encoded proteins after import into the mitochondrion. MPP belongs to a family of metalloendoproteases whose members include insulin-degrading enzymes from mammals and protease III from bacteria. Mammalian and fungal MPP are soluble heterodimers of α- and β-subunits localized in the mitochondrial matrix. Both subunits of MPP are required for the protease activity, but the active site is part of the β-subunit. The core-1 protein of the bovine bc_1 complex has 56% sequence identity to the β-subunit of rat MPP, 38% to yeast, and 42% to potato, whereas the core-2 protein is 27% identical to the α-subunit of rat MPP, 28% to yeast, and 30% to potato. Interestingly, the sequence identity of the bovine core proteins to the related MPP subunits of yeast is significantly higher than that of the yeast subunits itself [19]. We can therefore expect that the MPPs of these species are similar in structure to the bovine core-1 and core-2 subunits. In plant mitochondria, the MPP activity is membrane-bound and is an integral part of the bc_1 complex [2].

The bovine core-1 features a inversed putative Zn-binding motif consisting of two α helices (αA and αD, Fig. 5E) with a modified zinc-binding sequence of ^{BT}Y57XXE60H61-$(X)_{75}$-E137, compared to the consensus sequence of HXXEH-$(X)_{74\text{-}76}$-E [102]. In yeast, the motif has a rather different sequence of ^{Sc}N70XXK73N74-$(X)_{63}$-Q137. In addition, the yeast subunit lacks the loop ^{Sc}F64–N73 of its bovine homologue. With the rather conserved zinc-binding motif in the bovine core-1 subunit, it was expected that the heterodimeric core-1 and core-2 may possess proteolytic activity when it is freed from the bc_1 complex. Indeed, the core-1 and core-2 heterodimer of bovine bc_1, when treated with triton X-100, displays MPP activity that is divalent metal ion dependent [99] and inhibited by N-terminal signal peptide of the ISP precursor [3].

The dimeric core subunits are anchored to the membrane by recruiting peptide fragments from the N-terminus of subunit 7 and C-terminus of the cyt c_1 subunit and incorporating the two peptides into the β sheet in the N-terminal portion of the core-1 subunit (Fig. 5F). Additionally, the N-terminal peptide of the ISP subunit stays in close proximity to the crevice between core-1 and core-2, making additional contacts with the core-1 subunit.

5.2. Structures of other supernumerary subunits

In addition to the two core subunits, smaller supernumerary subunits have also been resolved in various crystal structures. For the bovine complex, structures of all eleven subunits were determined, whereas subunit 11 in avian structures and subunit QCR10, the

equivalent of subunit 11 in bovine bc_1, in yeast is missing (Table 1). Genetic and biochemical characterizations of supernumerary subunits were often carried out in yeast, illuminating some of their biological functions.

Subunit 6 (also named QPK, 13.4 *kDa*, QCR7 in yeast) was shown to be on the matrix side of the membrane. It is entirely helical and consists of four helices with connecting loops (Fig. 6A). It attaches on the matrix side to exposed residues of helices F, G, and H of one cyt *b* subunit in one monomer, while also making contact with core-1 and core-2 of the symmetry-related monomer (Fig. 1A). Because of its position in the bc_1 complex, this subunit is conceivably necessary to shield the Q_N pocket of the cyt *b* subunit from exposure to the aqueous environment on the matrix side, as partial removal of subunit 6 by proteolysis decouples redox-linked proton pumping [103].

Subunit 7 (also named QPC, 9.6 *kDa*, QCR8 in yeast) was identified as a quinol-binding protein, as it forms adducts with various azido-ubiquinone derivatives [104]. In yeast, mutagenesis of QCR8 indicated an important role of this subunit in the assembly of a functional enzyme and in inhibitor myxothiazol binding, suggesting an impaired Q_P site [105, 106]. The crystal structure shows that subunit 7 contributes to both the matrix and TM regions. The C-terminal 50 residues of subunit 7 form a long, bent TM helix, and its N-terminal part associates with the core-1 protein as part of a β sheet (Figs. 6B and 5F), serving as one of the membrane anchors for the subunits in the matrix region. The TM portion of the subunit is in direct contact with TM helices G and H of the cyt *b* subunit, forming a hydrophobic depression that could interact with hydrophobic molecules such as ubiquinone.

Subunit 8 (also called hinge-protein, 9.2 *kDa*, QCR6 in yeast) was previously thought to support ET from cyt c_1 to cyt *c* by mediating contacts between the two components. This is the only supernumerary subunit that is located on the positive side of the membrane. Crystal structures have confirmed its location and its interaction with the cyt c_1 subunit. Subunit 8 is entirely helical, consisting of three helices (Fig. 6C); it forms a hairpin like structure, which is stabilized by a couple of disulfide bonds. The subunit is highly acidic with a large number of glutamate and aspartate residues. In the structure, it exclusively interacts with the cyt c_1 subunit (Fig. 1A). Interestingly, in the yeast structure of bc_1 complexed with cyt *c*, subunit QCR6 is not in direct contact with the substrate, calling into question the idea that this subunit mediates interaction between cyt c_1 and cyt *c*.

Subunit 9 (8 *kDa*) is the signal peptide from the ISP precursor after proteolytic processing, and thus may have a role in incorporating the ISP subunit into the bc_1 complex. It has also been hypothesized that during assembly of the bc_1 complex, the ISP precursor protein may be used to recruit the heterodimeric core proteins as a suicide bait [99]. However, this subunit is not present in the yeast bc_1. In the crystal structure, subunit 9 is mostly associated with the core-2 subunit. The structure of subunit 9 is in large part a random coil with a pair of β-strands (Fig. 6D) that extends a β-sheet of core-2. A part of the subunit falls into the crevice between core-1 and core-2 and the modeled C-terminus of subunit 9 is not close to the N-terminus of the ISP subunit. From a crystallographic point of view, this subunit falls into the category of the least well-determined portion of the bc_1 structure.

Subunit 10 (7.2 *kDa*, QCR9 in yeast) is also called the cyt c_1 associated protein. Deletion of QCR9 in yeast leads to poor growth on non-fermentable carbon sources and the yeast exhibited very low wild-type bc_1 activity [107]. These results indicate that QCR9 is required for formation of a fully functional complex. The crystal structure of bc_1 revealed that subunit 10 is made of two helices: the N-terminal helix runs parallel to the negative side of

membrane surface, the middle helix is transmembrane, and its C-terminus extension reaches out to interact with cyt c_1 on the positive side of the membrane (Fig. 6E and Fig. 1A).

Subunit 11 (6.3 *kDa*, QCR10 in yeast) is preserved in the crystal structure of *Btbc*$_1$ but is not seen in those of avian and yeast, presumably due to different purification or crystallization procedures. This subunit features a single TM helix (Fig. 6F) that attaches perhaps loosely to the periphery of the complex.

6. Concluding remarks

Fifteen years have passed since the beginning of an era of crystal structure determination of *bc*$_1$, which not only beautifully illustrated the architecture of this integral membrane protein and confirmed the essence of the Q-cycle, it has also surprised us with structural features that was previously inaccessible using various experimental methods and shed new light on the mechanisms of *bc*$_1$ function and its inhibition. Crystallographic method has once again demonstrated its power in providing atomic resolution snap shots of *bc*$_1$ trapped as various reaction intermediates, which were necessary for reconstructing the reaction sequence of *bc*$_1$ function. Understanding the exact sequence of events during substrate processing holds the valuable promise of providing insight into processes of aging, mitochondrial diseases, apoptosis, pest control and possibly other phenomena.

Acknowledgments

We thank George Leiman for editorial assistance during the preparation of this manuscript. This research was supported in part by the Intramural Research Program of the NIH, National Cancer Institute, Center for Cancer Research, and in part from an NIH grant (GM 30721) to CAY.

Abbreviations

***bc*$_1$**	complex III or ubiquinol cytochrome *c* oxidoreductase or cytochrome *bc*$_1$
***b*$_L$**	low-potential heme or *b*$_{566}$
***b*$_H$**	high-potential heme or *b*$_{562}$
***Btbc*$_1$**	*Bos taurus bc*$_1$
CA	contact area
CL	cardiolipin
ET	electron transfer
***Ggbc*$_1$**	*Gallus gallus bc*$_1$
ISC	iron-sulfur cluster
ISP	iron-sulfur protein
ISP-ED	extrinsic domain of ISP
MPP	mitochondrial processing peptidase
***Mtbc*$_1$**	mitochondrial *bc*$_1$
NCS	Non-crystallographic symmetry
PDB	protein data bank
PC	phosphatidylcholine
PE	phosphatidylethanolamine

PI	phosphatidylinositol
rms deviation	root-mean-square deviation
Q_N	ubiquinone reduction
Q_P	ubiquinol oxidation
***Rsbc*$_1$**	bc_1 from *Rhodobacter sphaeroides*
SC	surface complementarity
***Scbc*$_1$**	bc_1 from *Saccharomyces cerevisiae*
TM	transmembrane
QH_2	ubiquinol
Q	ubiquinone

References

[1]. Trumpower BL, Gennis RB. Energy transduction by cytochrome complexes in mitochondrial and bacterial respiration: the enzymology of coupling electron transfer reactions to transmembrane proton translocation. Annual Review of Biochemistry. 1994; 63:675–716.

[2]. Glaser E, Eriksson A, Sjoling S. Bifunctional role of the bc1 complex in plants. Mitochondrial bc1 complex catalyses both electron transport and protein processing. FEBS Lett. 1994; 346:83–87. [PubMed: 8206164]

[3]. Deng K, Shenoy SK, Tso S, Yu L, Yu CA. Reconstitution of Mitochondrial Processing Peptidase from the Core Proteins (Subunits I and II) of Bovine Heart Mitochondrial Cytochrome bc1 Complex. Journal of Biological Chemistry. 2001; 276:6499–6505. [PubMed: 11073949]

[4]. Turrens JF, Alexandre A, Lehninger AL. Ubisemiquinone is the electron donor for superoxide formation by complex III of heart mitochondria. Archives of Biochemistry and Biophysics. 1985; 237:408–414. [PubMed: 2983613]

[5]. Yin Y, Yang S, Yu L, Yu CA. Reaction mechanism of superoxide generation during ubiquinol oxidation by the cytochrome bc1 complex. J Biol Chem. 2010; 285:17038–17045. [PubMed: 20371599]

[6]. Wenz T, Covian R, Hellwig P, Macmillan F, Meunier B, Trumpower BL, Hunte C. Mutational analysis of cytochrome b at the ubiquinol oxidation site of yeast complex III. J Biol Chem. 2007; 282:3977–3988. [PubMed: 17145759]

[7]. Lee DW, Selamoglu N, Lanciano P, Cooley JW, Forquer I, Kramer DM, Daldal F. Loss of a conserved tyrosine residue of cytochrome b induces reactive oxygen species production by cytochrome BC1. J Biol Chem. 2011

[8]. Tormos KV, Anso E, Hamanaka RB, Eisenbart J, Joseph J, Kalyanaraman B, Chandel NS. Mitochondrial complex III ROS regulate adipocyte differentiation. Cell Metab. 2011; 14:537–544. [PubMed: 21982713]

[9]. Keilin D. Proc. R. Soc. Lond. 1925; B98:312–399.

[10]. Hatefi Y, Haavik AG, Griffiths DE. Studies on the Electron Transfer System: XLI Reduced Co-enzyme Q (QH2-cytochrome c reductase). Journal of Biological Chemistry. 1962; 237:1681–1685. [PubMed: 13905328]

[11]. Tzagoloff A, Yang PC, Wharton DC, Rieske JS. Studies of the electron-transfer system. LXIV. Role of phospholipid in cytochrome oxidase. Biochimica et Biophysica Acta. 1965; 96:1–8. [PubMed: 14285264]

[12]. Xia D, Yu CA, Kim H, Xia JZ, Kachurin AM, Zhang L, Yu L, Deisenhofer J. Crystal structure of the cytochrome bc1 complex from bovine heart mitochondria. Science. 1997; 277:60–66. [PubMed: 9204897]

[13]. Ljungdahl PO, Pennoyer JD, Robertson DE, Trumpower BL. Purification of highly active cytochrome bc1 complexes from phylogenetically diverse species by a single chromatophaphic procedure. Biochimica et Biophysica Acta. 1987; 891:227–241. [PubMed: 3032252]

[14]. Yu CA, Yu L. Structural role of phospholipids in ubiquinol-cytochrome c reductase. Biochemistry. 1980; 19:5715–5720. [PubMed: 6257287]

[15]. Link TA, Saynovits M, Assmann C, Iwata S, Ohnishi T, von Jagow G. Isolation, characterisation and crystallisation of a water-soluble fragment of the Rieske iron-sulfur protien of bovine heart mitochondrial bc1 complex. European Journal of Biochemistry. 1996; 237:71–75. [PubMed: 8620896]

[16]. Iwata S, Saynovits M, Link TA, Michel H. Structure of a water soluble fragment of the 'Rieske' iron-sulfur protein of the bovine heart mitochondrial cytochrome bc1 complex determined by MAD phasing at 1.5 A resolution. Structure. 1996; 4:567–579. [PubMed: 8736555]

[17]. Iwata S, Lee JW, Okada K, Lee JK, Iwata M, Rasmussen B, Link TA, Ramaswamy S, Jap BK. Complete structure of the 11-subunit bovine mitochondrial cytochrome bc1 complex [see comments]. Science. 1998; 281:64–71. [PubMed: 9651245]

[18]. Zhang Z, Huang L, Shulmeister VM, Chi YI, Kim KK, Hung LW, Crofts AR, Berry EA, Kim SH. Electron transfer by domain movement in cytochrome bc1. Nature. 1998; 392:677–684. [PubMed: 9565029]

[19]. Hunte C, Koepke J, Lange C, Rossmanith T, Michel H. Structure at 2.3 A resolution of the cytochrome bc(1) complex from the yeast Saccharomyces cerevisiae co-crystallized with an antibody Fv fragment. Structure. 2000; 15:669–684. [PubMed: 10873857]

[20]. Berry EA, Huang L, Saechao LK, Pon NG, Valkova-Valchanova M, Daldal F. X-ray structure of Rhodobacter capsulatus cytochrome bc1: comparison with its mitochondrial and chloroplast counterparts. Photosynthesis Research. 2004; 81:251–275. [PubMed: 16034531]

[21]. Esser L, Elberry M, Zhou F, Yu CA, Yu L, Xia D. Inhibitor complexed structures of the cytochrome bc1 from the photosynthetic bacterium Rhodobacter sphaeroides at 2.40 Å resolution. J Biol Chem. 2008; 283:2846–2857. [PubMed: 18039651]

[22]. Kleinschroth T, Castellani M, Trinh CH, Morgner N, Brutschy B, Ludwig B, Hunte C. X-ray structure of the dimeric cytochrome bc(1) complex from the soil bacterium Paracoccus denitrificans at 2.7-A resolution. Biochim Biophys Acta. 2011; 1807:1606–1615. [PubMed: 21996020]

[23]. Smith JL, Zhang H, Yan J, Kurisu G, Cramer WA. Cytochrome bc complexes: a common core of structure and function surrounded by diversity in the outlying provinces. Curr Opin Struct Biol. 2004; 14:432–439. [PubMed: 15313237]

[24]. Palsdottir H, Lojero CG, Trumpower BL, Hunte C. Structure of the yeast cytochrome bc1 complex with a hydroxyquinone anion Qo site inhibitor bound. Journal of Biological Chemistry. 2003; 278:31303–31311. [PubMed: 12782631]

[25]. Xia D, Esser L, Elberry M, Zhou F, Yu L, Yu CA. The road to the crystal structure of the cytochrome bc1 complex from the anoxigenic, photosynthetic bacterium Rhodobacter sphaeroides. J Bioenerg Biomembr. 2008; 40:485–492. [PubMed: 18953640]

[26]. Gao X, Wen X, Yu C, Esser L, Tsao S, Quinn B, Zhang L, Yu L, Xia D. The crystal structure of mitochondrial cytochrome bc1 in complex with famoxadone: the role of aromatic-aromatic interaction in inhibition. Biochemistry. 2002; 41:11692–11702. [PubMed: 12269811]

[27]. Gao X, Wen X, Esser L, Yu L, Yu CA, Xia D. Structural basis for the quinone reduction in bc1 complex: a comparative analysis of crystal structures of mitochondrial cytochrome bc1 with bound substrate and inhibitors. Biochemistry. 2003; 42:9067–9080. [PubMed: 12885240]

[28]. Leonard K, Wingfield P, Arad T, Weiss H. Three-dimensional structure of ubiquinol:cytochrome c reductase from Neurospora mitochondria determined by electron microscopy of membrane crystals. Journal of Molecular Biology. 1981; 149:259–274. [PubMed: 6273583]

[29]. Akiba T, Toyoshima C, Matsunaga T, Kawamoto M, Kubota T, Fukuyama K, Namba K, Matsubara H. Three-Dimensional Structure of Bovine Cytochrome bc1 Complex By Electron Cryomicroscopy and Helical Image Reconstruction. Nature Structural Biology. 1996; 3:553–561.

[30]. Schagger H, Link TA, Engel WD, von Jagow G. Isolation of the eleven protein subunits of the bc1 complex from beef heart. Methods in Enzymology. 1986; 126:224–237. [PubMed: 2856130]

[31]. Farid RS, Moser CC, Dutton PL. Electron transfer in proteins. Current Opinion in Structural Biology. 1993; 3:225–233.

[32]. Kim H, Xia D, Yu CA, Xia JZ, Kachurin AM, Zhang L, Yu L, Deisenhofer J. Inhibitor binding changes domain mobility in the iron-sulfur protein of the mitochondrial bc1 complex from bovine heart. Proceedings of National Academy of Sciences.U.S.A. 1998; 95:8026–8033.

[33]. Degli Esposti M, De Vries S, Crimi M, Ghelli A, Patarnello T, Meyer A. Mitochondrial Cytochrome b: evolution and structure of the protein. Biochim.Biophys.Acta. 1993; 1143:243–271. [PubMed: 8329437]

[34]. Gong X, Yu L, Yu CA. The role of an extra fragment of cytochrome b (residues 309-326) in the cytochrome bc1 complex from Rhodobacter sphaeroides. Biochemistry. 2006; 45:11122–11129. [PubMed: 16964973]

[35]. Elberry M, Yu L, Yu CA. The disulfide bridge in the head domain of Rhodobacter sphaeroides cytochrome c1 is needed to maintain its structural integrity. Biochemistry. 2006; 45:4991–4997. [PubMed: 16605267]

[36]. Osyczka A, Dutton PL, Moser CC, Darrouzet E, Daldal F. Controlling the functionality of cytochrome c(1) redox potentials in the Rhodobacter capsulatus bc(1) complex through disulfide anchoring of a loop and a beta-branched amino acid near the heme-ligating methionine. Biochemistry. 2001; 40:14547–14556. [PubMed: 11724568]

[37]. Xiao K, Liu X, Yu CA, Yu L. The extra fragment of the iron-sulfur protein (Residues 96-107) of Rhodobacter sphaeroides cytochrome bc1 complex is required for protein stability. Biochemistry. 2004; 43:1488–1495. [PubMed: 14769025]

[38]. Mitchell P. Possible molecular mechanisms of the protonmotive function of cytochrome systems. Journal of Theoretical Biology. 1976; 62:327–367. [PubMed: 186667]

[39]. Trumpower BL. The protonmotive Q cycle. Energy transduction by coupling of proton translocation to electron transfer by the cytochrome bc1 complex. Journal of Biological Chemistry. 1990; 265:11409–11412. [PubMed: 2164001]

[40]. Wikstrom MK, Berden JA. Oxidoreduction of cytochrome b in the presence of antimycin. Biochim.Biophys.Acta. 1972; 283:403–420. [PubMed: 4346389]

[41]. Erecinska M, Chance B, Wilson DF, Dutton PL. Aerobic reduction of cytochrome b 566 in pigeon-heart mitochondria (succinate-cytochrome C1 reductase-stopped-flow kinetics). Proceedings of National Academy of Sciences.U.S.A. 1972; 69:50–54.

[42]. Trumpower BL, Edwards CA. Identification of Oxidation Factor as a Reconstitutively Active Form of the Iron-Sulfur Protein of the Cytochrome b-c1 Segment of the Respiratory Chain. FEBS Letters. 1979; 100:13–16. [PubMed: 220085]

[43]. Brand MD, Reynafarje B, Lehninger AL. Re-evaluation of the H+/site ratio of mitochondrial electron transport with the oxygen pulse technique. Journal of Biological Chemistry. 1976; 251:5670–5679. [PubMed: 9396]

[44]. Hendler RW, Bunow B, Rieske JS. Thermodynamic and kinetic considerations of Q-cycle mechanisms and the oxidant-induced reduction of cytochromes b. Journal of Bioenergetics and Biomembranes. 1985; 17:51–64. [PubMed: 3988725]

[45]. Brandt U, von Jagow G. Analysis of inhibitor binding to the mitochondrial cytochrome c reductase by fluorescence quench titration. European Journal of Biochemistry. 1991; 195:163–170. [PubMed: 1991466]

[46]. Ding H, Robertson DE, Daldal F, Dutton PL. Cytochrome bc1 complex [2Fe-2S] cluster and its interaction with ubiquinone and ubihydroquinone at the Qo site: A double-occupancy Qo site model. Biochemistry. 1992; 31:3144–3158. [PubMed: 1313287]

[47]. Brandt U. Bifurcated ubihydroquinone oxidation in the cytochrome bc1 complex by proton-gated charge transfer. FEBS Lett. 1996; 387:1–6. [PubMed: 8654557]

[48]. Rich PR. The quinone chemistry of bc complexes. Biochim Biophys Acta. 2004; 1658:165–171. [PubMed: 15282188]

[49]. Crofts AR, Wang Z. How rapid are the internal reactions of the ubiquinol:cytochrome c2 oxidoreductase? Photosynthesis Research. 1989; 22:69–87.

[50]. Cape JL, Bowman MK, Kramer DM. A semiquinone intermediate generated at the Qo site of the cytochrome bc1 complex: importance for the Q-cycle and superoxide production. PNAS. 2007; 104:7887–7892. [PubMed: 17470780]

[51]. Crofts AR, Meinhardt SW, Jones KR, Snozzi M. The Role of the Quinone Pool in the Cyclic Electron-Transfer Chain of Rhodopseudomonas Sphaeroides: A Modified Q-Cycle Mechanism. Biochim Biophys Acta. 1983; 723:202–218. [PubMed: 21494412]

[52]. Zhu J, Egawa T, Yeh S, Yu L, Yu CA. Simultaneous reduction of iron-sulfur protein and cytochrome bL during ubiquinol oxidation in cytochrome bc1 complex. PNAS. 2007; 104:4864–4869. [PubMed: 17360398]

[53]. Covian R, Trumpower BL. The rate-limiting step in the cytochrome bc1 complex (Ubiquinol-Cytochrome c Oxidoreductase) is not changed by inhibition of cytochrome b-dependent deprotonation: implications for the mechanism of ubiquinol oxidation at center P of the bc1 complex. J Biol Chem. 2009; 284:14359–14367. [PubMed: 19325183]

[54]. Berry EA, Huang L. Observations concerning the quinol oxidation site of the cytochrome bc1 complex. FEBS Lett. 2003; 555:13–20. [PubMed: 14630312]

[55]. Osyczka A, Moser CC, Dutton PL. Fixing the Q cycle. Trends in biochemical sciences. 2005; 30:176–182. [PubMed: 15817393]

[56]. Crofts AR, Lhee S, Crofts SB, Cheng J, Rose S. Proton pumping in the bc1 complex: a new gating mechanism that prevents short circuits. Biochim Biophys Acta. 2006; 1757:1019–1034. [PubMed: 16600173]

[57]. Esser L, Gong X, Yang S, Yu L, Yu CA, Xia D. Surface-modulated motion switch: capture and release of iron-sulfur protein in the cytochrome bc1 complex. Proc Natl Acad Sci U S A. 2006; 103:13045–13050. [PubMed: 16924113]

[58]. Esser L, Quinn B, Li Y, Zhang M, Elberry M, Yu L, Yu CA, Xia D. Crystallographic studies of quinol oxidation site inhibitors: A modified classification of inhibitors for the cytochrome bc1 complex. Journal of Molecular Biology. 2004; 341:281–302. [PubMed: 15312779]

[59]. Mulkidjanian AY. Ubiquinol oxidation in the cytochrome bc1 complex: reaction mechanism and prevention of short-circuiting. Biochim Biophys Acta. 2005; 1709:5–34. [PubMed: 16005845]

[60]. Nett JH, Hunte C, Trumpower BL. Changes to the length of the flexible linker region of the Rieske protein impair the interaction of ubiquinol with the cytochrome bc1 complex. Eur J Biochem. 2000; 267:5777–5782. [PubMed: 10971589]

[61]. Tian H, White S, Yu L, Yu CA. Evidence for the head domain movement of the Rieske iron-sulfur protein in electron transfer reaction of the cytochrome bc1 complex. Journal of Biological Chemistry. 1999; 274:7146–7152. [PubMed: 10066773]

[62]. Tian H, Yu L, Mather MW, Yu CA. Flexibility of the neck region of the rieske iron-sulfur protein is functionally important in the cytochrome bc1 complex. Journal of Biological Chemistry. 1998; 273:27953–27959. [PubMed: 9774409]

[63]. Xiao K, Yu L, Yu CA. Confirmation of the involvement of protein domain movement during the catalytic cycle of the cytochrome bc1 complex by the formation of the intersubunit disulfide bond between cytochrome b and the iron-sulfur protein. Journal of Biological Chemistry. 2000; 275:38597–38604. [PubMed: 10978350]

[64]. Darrouzet E, Valkova-Valchanova M, Daldal F. Probing the role of the Fe-S subunit hinge region during Q(o) site catalysis in Rhodobacter capsulatus bc(1) complex. Biochemistry. 2000; 39:15475–15483. [PubMed: 11112533]

[65]. Darrouzet E, Moser CC, Dutton PL, Daldal F. Large scale domain movement in cytochrome bc(1): a new device for electron transfer in proteins. Trends in biochemical sciences. 2001; 26:445–451. [PubMed: 11440857]

[66]. Brugna M, Rodgers S, Montoya G, Kazmeier M, Nitschke W, Sinning I. A spectroscopic method for observing the domain movement of the Rieske iron-sulfur protein. Proceedings of National Academy of Sciences.U.S.A. 2000; 97:2069–2074.

[67]. Obungu VH, Wang Y, Amyot SM, Gocke CB, Beattie DS. Mutations in the tether region of the iron-sulfur protein affect the activity and assembly of the cytochrome bc(1) complex of yeast mitochondria. Biochim Biophys Acta. 2000; 1457:36–44. [PubMed: 10692548]

[68]. Sadoski RC, Engstrom G, Tian H, Zhang L, Yu CA, Yu L, Durham B, Millett F. Use of a photoactivated ruthenium dimer complex to measure electron transfer between the Rieske iron-sulfur protein and cytochrome c(1) in the cytochrome bc(1) complex. Biochemistry. 2000; 39:4231–4236. [PubMed: 10757970]

[69]. Engstrom G, Xiao K, Yu CA, Yu L, Durham B, Millett F. Photoinduced electron transfer between the Rieske iron-sulfur protein and cytochrome c(1) in the Rhodobacter sphaeroides cytochrome bc(1) complex. Effects of pH, temperature, and driving force. J Biol Chem. 2002; 277:31072–31078. [PubMed: 12045199]

[70]. Gurung B, Yu L, Xia D, Yu CA. The iron-sulfur cluster of the Rieske iron-fulfur protein functions as a proton-exiting gate in teh cytochrome bc(1) complex. Journal of Biological Chemistry. 2005; 280:24895–24902. [PubMed: 15878858]

[71]. Berry EA, Huang LS. Conformationally linked interaction in the cytochrome bc(1) complex between inhibitors of the Q(o) site and the Rieske iron-sulfur protein. Biochim Biophys Acta. 2011; 1807:1349–1363. [PubMed: 21575592]

[72]. Yu CA, Wen X, Xiao K, Xia D, Yu L. Inter- and intra-molecular electron transfer in the cytochrome bc1 complex. Biochim.Biophys.Acta. 2002; 1555:65–70. [PubMed: 12206893]

[73]. Xia D, Esser L, Tang WK, Zhang M, Yu L, Yu CA. Redox coupled conformational changes in cytochrome bc1 compex: implication to the bifucated electron transfer at the quinol oxidation site. Biophys J. 2010; 100:3a.

[74]. Degli Esposti M, Crimi M, Ghelli A. Natural variation in the potency and binding sites of mitochondrial quinone-like inhibitors. Biochemical Society Transactions. 1993; 22:209–213. [PubMed: 8206230]

[75]. Tian H, Yu L, Mather MW, Yu CA. The Involvement of Serine 175 and Alanine 185 of Cytochrome b of Rhodobacter sphaeroides Cytochrome bc1 Complex in Interaction with Iron-Sulfur Protein. Journal of Biological Chemistry. 1997; 272:23722–23728. [PubMed: 9295316]

[76]. Xia D, Esser L, Yu L, Yu CA. Structural basis for the mechanism of electron bifurcation at the quinol oxidation site of the cytochrome bc1 complex. Photosynthesis Research. 2007; 92:17–34. [PubMed: 17457691]

[77]. Hansen KC, Schultz BE, Wang G, Chan SI. Reaction of Escherichia coli cytochrome bo3 and mitochondrial cytochrome bc1 with a photoreleasable decylubiquinol. Biochimica et Biophysica Acta. 2000; 1456:121–137. [PubMed: 10627300]

[78]. Bowyer JR, Crofts AR. On the mechanism of photosynthetic electron transfer in Rhodopseudomonas capsulata and Rhodopseudomonas sphaeroides. Biochim Biophys Acta. 1981; 636:218–233. [PubMed: 6269602]

[79]. Gopta OA, Feniouk BA, Junge W, Mulkidjanian AY. The cytochrome bc1 complex of Rhodobacter capsulatus: ubiquinol oxidation in a dimeric Q-cycle? FEBS Letters. 1998; 431:291–296. [PubMed: 9708922]

[80]. Bruel C, di Rago J, Slonimski PP, Lemesle-Meunier D. Role of the evolutionarily conserved cytochrome b tryptophan 142 in the ubiquinol oxidation catalyzed by the bc1 complex in the yeast Saccharomyces cerevisiae. Journal of Biological Chemistry. 1995; 270:22321–22328. [PubMed: 7673215]

[81]. Rajagukguk S, Yang S, Yu CA, Yu L, Durham B, Millett F. Effect of mutations in the cytochrome b ef loop on the electron-transfer reactions of the Rieske iron-sulfur protein in the cytochrome bc(1) complex. Biochemistry. 2007; 46:1791–1798. [PubMed: 17253777]

[82]. Crofts, AR.; Barquera, B.; Bechmann, G.; Guergova, M.; Salcedo-Hernandez, R.; Hacker, B.; hong, S.; Gennis, RB.; Mathis, P. Photosynthesis: from light to biosphere. Kluwer Academic Publications; The Netherlands: 1995. p. 493-500.

[83]. Mather MW, Yu L, Yu CA. The involvement of threonine 160 of cytochrome b of Rhodobacter sphaeroides cytochrome bc1 complex in quinone binding and interaction with subunit IV. Journal of Biological Chemistry. 1995; 270:28668–28675. [PubMed: 7499386]

[84]. Ding H, Moser CC, Robertson DE, Tokito MK, Daldal F, Dutton PL. Ubiquinone pair in the Qo site central to the primary energy conversion reactions of cytochrome bc1 complex. Biochemistry. 1995; 34:15979–15996. [PubMed: 8519754]

[85]. Yu CA, Cen X, Ma HW, Yin Y, Yu L, Esser L, Xia D. Domain conformational switch of the iron-sulfur protein in cytochrome bc1 complex is induced by the electron transfer from cytochrome bL to bH. Biochim Biophys Acta. 2008; 1777:1038–1043. [PubMed: 18452702]

[86]. Cen X, Yu L, Yu CA. Domain movement of iron sulfur protein in cytochrome bc1 complex is facilitated by the electron transfer from cytochrome b(L) to b(H). FEBS Lett. 2008; 582:523–526. [PubMed: 18230359]

[87]. Lange C, Hunte C. Crystal structure of the yeast cytochrome bc1 complex with its bound substrate cytochrome c. PNAS. 2002; 99:1800–2805.

[88]. Solmaz SR, Hunte C. Structure of complex III with bound cytochrome c in reduced state and definition of a minimal core interface for electron transfer. J Biol Chem. 2008; 283:17542–17549. [PubMed: 18390544]

[89]. Gomez B Jr, Robinson NC. Phospholipase digestion of bound cardiolipin reversibly inactivates bovine cytochrome bc1. Biochemistry. 1999; 38:9031–9038. [PubMed: 10413476]

[90]. Schagger H, Hagen T, Roth B, Brandt U, Link TA, von Jagow G. Phospholipid specificity of bovine heart bc1 complex. Eur.J.Biochem. 1990; 190:123–130. [PubMed: 2163831]

[91]. Lange C, Nett JH, Trumpower BL, Hunte C. Specific roles of protein-phospholipid interactions in the yeast cytochrome bc1 complex structure. The EMBO Journal. 2001; 20:6591–6600. [PubMed: 11726495]

[92]. Wenz T, Hielscher R, Hellwig P, Schagger H, Richers S, Hunte C. Role of phospholipids in respiratory cytochrome bc(1) complex catalysis and supercomplex formation. Biochim Biophys Acta. 2009; 1787:609–616. [PubMed: 19254687]

[93]. von Jagow G, Link TA. Use of specific inhibitors on the mitochondrial bc1 complex. Methods in Enzymology. 1986; 126:253–271. [PubMed: 2856132]

[94]. Link TA, Haase U, Brandt U, von Jagow G. What information do inhibitors provide about the structure of the hydroquinone oxidation site of ubihydroquinone: cytochrome c oxidoreductase? Journal of Bioenergetics and Biomembrane. 1993; 25:221–232.

[95]. Yamashita E, Zhang H, Cramer WA. Structure of the cytochrome b6f complex: quinone analogue inhibitors as ligands of heme cn. J Mol Biol. 2007; 370:39–52. [PubMed: 17498743]

[96]. Berry EA, Zhang Z, Bellamy HD, Huang L. Crystallographic location of two Zn2+-binding sites in the avian cytochrome bc1 complex. Biochimica et Biophysica Acta. 2000; 1459:440–448. [PubMed: 11004461]

[97]. Lee DW, El Khoury Y, Francia F, Zambelli B, Ciurli S, Venturoli G, Hellwig P, Daldal F. Zinc inhibition of bacterial cytochrome bc(1) reveals the role of cytochrome b E295 in proton release at the Q(o) site. Biochemistry. 2011; 50:4263–4272. [PubMed: 21500804]

[98]. Lorusso M, Cocco T, Sardanelli AM, Minuto M, Bonomi F, Papa S. Interaction of Zn2+ with the bovine-heart mitochondrial bc1 complex. Eur J Biochem. 1991; 197:555–561. [PubMed: 1851092]

[99]. Deng K, Zhang L, Kachurin AM, Yu L, Xia D, Kim H, Deisenhofer J, Yu CA. Activation of a matrix processing peptidase from the crystalline cytochrome bc1 complex of bovine heart mitochondria. J Biol Chem. 1998; 273:20752–20757. [PubMed: 9694818]

[100]. Schoppink PJ, Hemrika W, Berden JA. the effect of deletion of the genes encoding the 40 kDa subunit II or the 17 kDa subunit VI on the steady-state kinetics of yeast ubiquinol-cytochrome-c oxidoreductase. Biochimica et Biophysica Acta. 1989; 974:192–201. [PubMed: 2540835]

[101]. Braun H, Emmermann M, Kruft V, Schmitz UK. The general mitochondrial processing peptidase from potato is an integral part of cytochrome c reductase of the respiratory chain. The EMBO Journal. 1992; 11:3219–3227. [PubMed: 1324169]

[102]. Becker AB, Roth RA. An unusual active site identified in a family of zinc metalloendopeptidases. Proc Natl Acad Sci U S A. 1992; 89:3835–3839. [PubMed: 1570301]

[103]. Cocco T, Lorusso M, Sardanelli AM, Minuto M, Ronchi S, Tedeschi G, Papa S. Structural and Functional Characteristics of Polypeptide Subunits of the Bovine Heart Ubiquinol-Cytochrome c Reductase Complex. Eur.J.Biochem. 1991; 195:731–734. [PubMed: 1847870]

[104]. Yu L, Yang FD, Yu CA. Interaction and identification of ubiquinone-binding proteins in ubiquinol-cytochrome c reductase by azido-ubiquinone derivatives. Journal of Biological Chemistry. 1985; 260:963–973. [PubMed: 2981854]

[105]. Hemrika W, Berden JA, Grivell LA. A region of the C-terminal part of the 11-kDa subunit of ubiquinol-cytochrome-c oxidoreductase of the yeast Saccharomyces cerevisiae contributes to the structure of the Qout reaction domain. Eur J Biochem. 1993; 215:601–609. [PubMed: 8394810]

[106]. Hemrika W, Lobo-Hajdu G, Berden JA, Grivell LA. The aromatic nature of residue 66 of the 11-kDa subunit of ubiquinol-cytochrome c oxidoreductase of the yeast Saccharomyces cerevisiae is important for the assembly of a functional enzyme. FEBS Lett. 1994; 344:15–19. [PubMed: 8181557]

[107]. Phillips JD, Graham LA, Trumpower BL. Subunit 9 of the Saccharomyces cerevisiae cytochrome bc1 complex is required for insertion of EPR-detectable iron-sulfur cluster into the Rieske iron-sulfur protein. J Biol Chem. 1993; 268:11727–11736. [PubMed: 8389362]

[108]. Berry EA, Zhang Z, Bellamy HD, Huang L. Crystallographic location of two Zn2+-binding sites in the avian cytochrome bc1 complex. Biochimica et Biophysica Acta (BBA) - Bioenergetics. 2000; 1459:440–448.

[109]. Gao X, Wen X, Esser L, Quinn B, Yu L, Yu CA, Xia D. Structural basis for the quinone reduction in the bc1 complex: a comparative analysis of crystal structures of mitochondrial cytochrome bc1 with bound substrate and inhibitors at the Qi site. Biochemistry. 2003; 42:9067–9080. [PubMed: 12885240]

[110]. Berry EA, Huang L-s, Lee D-W, Daldal F, Nagai K, Minagawa N. Ascochlorin is a novel, specific inhibitor of the mitochondrial cytochrome bc1 complex. Biochimica et Biophysica Acta (BBA) - Bioenergetics. 2010; 1797:360–370.

[111]. Crowley PJ, Berry EA, Cromartie T, Daldal F, Godfrey CRA, Lee D-W, Phillips JE, Taylor A, Viner R. The role of molecular modeling in the design of analogues of the fungicidal natural products crocacins A and D. Bioorganic & Medicinal Chemistry. 2008; 16:10345–10355. [PubMed: 18996700]

[112]. Huang LS, Cobessi D, Tung EY, Berry EA. Binding of the respiratory chain inhibitor antimycin to the mitochondrial bc1 complex: a new crystal structure reveals an altered intramolecular hydrogen-bonding pattern. Journal of Molecular Biology. 2005; 351:573–597. [PubMed: 16024040]

[113]. Lancaster CR, Hunte C, Kelley J 3rd, Trumpower BL, Ditchfield R. A comparison of stigmatellin conformations, free and bound to the photosynthetic reaction center and the cytochrome bc1 complex. J Mol Biol. 2007; 368:197–208. [PubMed: 17337272]

[114]. Althoff T, Mills DJ, Popot JL, Kuhlbrandt W. Arrangement of electron transport chain components in bovine mitochondrial supercomplex I1III2IV1. Embo J. 2011; 30:4652–4664. [PubMed: 21909073]

Highlights

- Crystal structures of cyt bc1 complexes have been determined from diverse organisms
- ISP-ED undergoes binary conformational changes upon binding of different inhibitors
- ISP-ED conformation is controlled by modulating its binding affinity to cyt b subunit
- Bifurcated ET can be explained by the “Surface-affinity modulated ISP motion switch hypothesis”
- This mechanism has received substantial experimental support

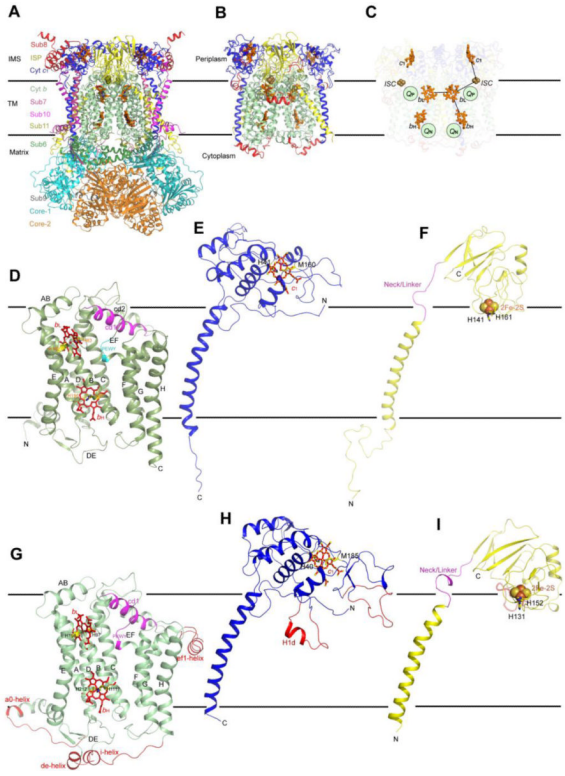

Figure 1. Crystal structures in ribbon representation for mitochondrial and bacterial bc_1 complexes

(A) Structural model of the dimeric bc_1 complex from bovine mitochondria. The eleven different subunits are represented as ribbons with the color codes and subunit designations given on the left. Prosthetic groups such as the hemes b_L, b_H, and c_1 are shown as stick models. The Iron-sulfur clusters are shown as van der Waals sphere models. The two black horizontal lines delineate the boundaries of the membrane bilayer. The three regions of the bc_1 complex are indicated as IMS (intermembrane space), TM (transmembrane) and Matrix regions, respectively. (B) Structural model of the photosynthetic bacterium *R. sphaeroides* bc_1. Color codes for $Rsbc_1$ are the same as those for $Btbc_1$ except those in red, which represent insertions in cyt *b*, cyt c_1 and ISP subunits in relation to the corresponding subunits in $Btbc_1$. (C) Positions of and distances between iron atoms of prosthetic groups. Hemes b_L, b_H and c_1 as well as 2Fe-2S clusters are labeled. Arrowed lines indicate low and high potential chains for ET. (D) Ribbon diagram showing the structure of monomeric bovine cyt *b*. Eight TM helices are labeled. The two *b*-type hemes b_L and b_H are shown as stick models. The axial histidine ligands to the heme groups are also shown as stick models and labeled. The two conserved and functionally important motifs, the cd1 helix and the PEWY sequence, are shown in magenta and cyan, respectively, and as labeled. (E) Ribbon presentation of the structure of bovine cyt c_1. *Bt*cyt c_1 has its N- and C-terminus on the positive and negative sides of the membrane, respectively. The heme c_1 along with its two axial ligands ^{Bt}M160 and ^{Bt}H41 are shown as stick models. (F) Ribbon diagram showing the structure of the bovine ISP subunit. The N-terminus of the ISP is on the negative side of the membrane, whereas the C-terminus is on the positive side. The 2Fe-2S cluster is shown as spheres; the two histidine ligands H141 and H161 for the ISC are shown as stick models and are labeled. The flexible linker or neck between the TM helix and the ISP-ED is shown as a loop in magenta. (G) Ribbon diagram of the structure of *Rs*cyt *b*. Structural features of the subunit are similarly labeled as those in *Bt*cyt *b* except for the insertions, which are shown in red. Histidine ligands to the hemes b_L (H97 and H198) and to b_H (H111 and H212) are

shown as stick models. (H) Ribbon representation of the structure of *Rs*cyt c_1. Structural features of the subunit are similarly labeled as those in *Bt*cyt c_1 except for the insertions, which are shown in red. Heme c_1 ligands are given as stick models for M185 and H40. (I) Ribbon diagram showing the structure of *Rs*ISP. Structural features of the subunit are similarly labeled as those in *Bt*ISP except for the insertions, which are shown in red. Histidine ligands to the *Rs*ISC are show as stick models for H131 and H152.

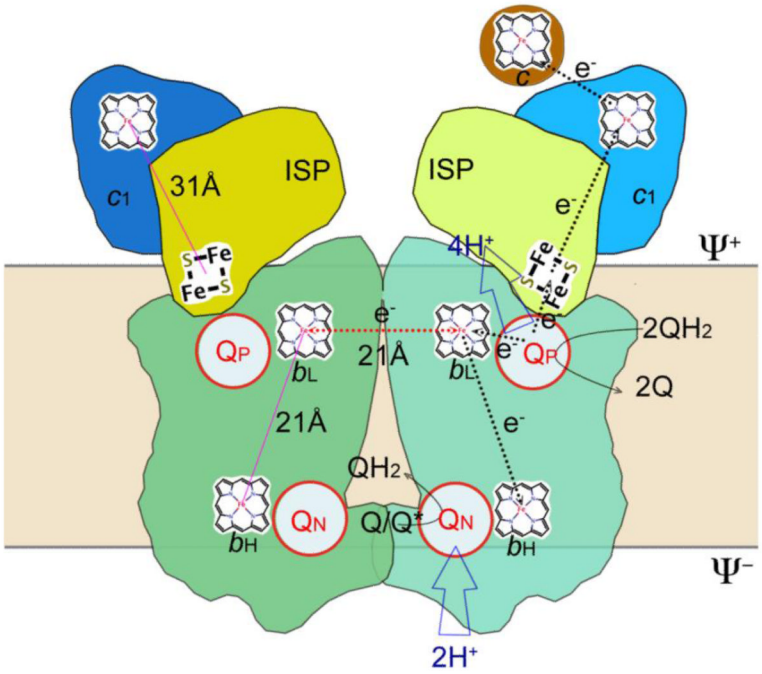

Figure 2. Q-cycle mechanism

The Q cycle mechanism defines two reaction sites: quinol oxidation (Center P or Q_P) and quinone reduction (Center N or Q_N). It takes two quinol oxidation cycles to complete. At first, a QH_2 moves into the Q_P site and undergoes oxidation with one electron going to cyt *c* via the ISP and cyt c_1 (high-potential chain), and another ending in the Q_N via hemes b_L and b_H (low-potential chain) to form a ubisemiquinone, and releasing its two protons to the Φ^+ site of the membrane. The second QH_2 is oxidized in the same way at the Q_P site but its low potential chain electron ends up reducing the ubisemiquinone radical. Reduced QH_2 is released upon picking up two protons from the negative side of the membrane. As a result of the Q cycle, 4 protons are transferred to the Φ^+ side, 2 protons are picked up from the Φ^- side and effectively only one QH_2 molecule is oxidized.

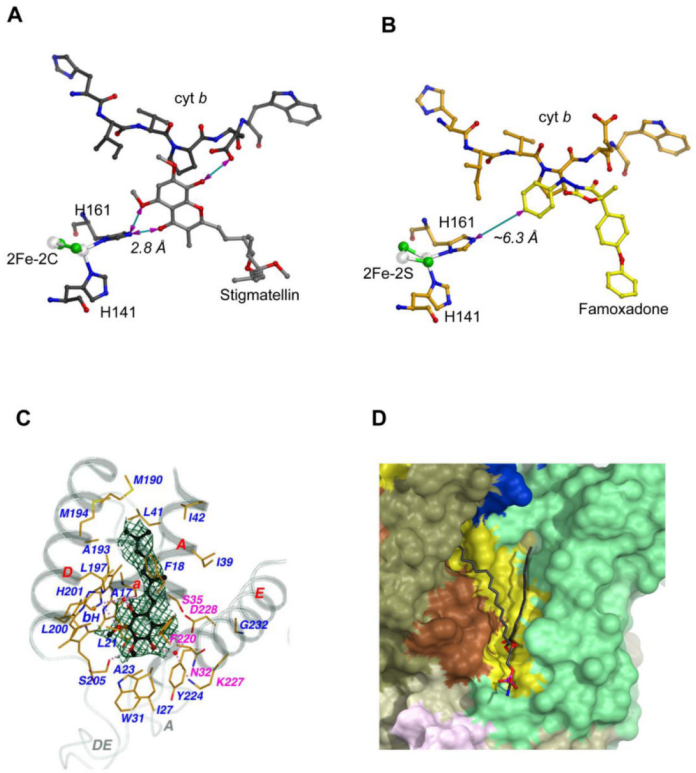

Figure 3. Binding of substrate, inhibitor and lipid molecules to the cyt bc_1 complex

(A) Hydrogen bonding interaction between stigmatellin and the ISP. In this figure, much of the protein structures of cyt *b* and ISP are omitted for clarity to illustrate the H-bond between stigmatellin and the ISC. All residues, the ISC, and stigmatellin are shown as ball-and-stick models and as labeled. The distance between ^{BT}H161, one of the 2Fe-2S ligand, and stigmatellin is shown as 2.8 Å. (B) No hydrogen bonding is observed between famoxadone and the ISP. Binding of famoxadone arrests the ISP-ED motion. But the closest distance between ^{BT}H161 and the ISP is >6 Å. (C) Interaction of the protein environment at the Q_N site of the cyt *b* subunit with bound substrate ubiquinone with two isoprenoid repeats. Secondary structure elements surrounding the Q_N pocket, including portions of the N-terminal helix a, TM helices A, D, and E, and extra-membrane loops A and DE, are shown and are labeled. Residues interacting with bound substrate and the b_H heme are drawn in stick models and are labeled with carbon atoms in yellow, nitrogen in blue, oxygen in red, and iron in orange. H-bonds are indicated with pinkish dotted lines. Water molecules are shown as isolated red balls. The residues that are with magenta labels confer inhibitor resistance. The substrate ubiquinone, caged in *F*o-*F*c electron densities calculated with refined phases after ligand being omitted and contoured at the 3σ level in dark green, are drawn as ball-and-stick models with carbon atoms in black, nitrogen in light blue, and oxygen in red. Additionally, the two bound water molecules are enclosed in the *F*o-*F*c electron density in cyan calculated with refined phases obtained with the waters omitted and contoured at 3σ. (D) Binding environment of the bound lauryl oleoyl phosphatidyl ethanolamine (PE) in the structure of *Rsbc*$_1$. The modeled lipid is located near the N-side and its binding environment is shown.

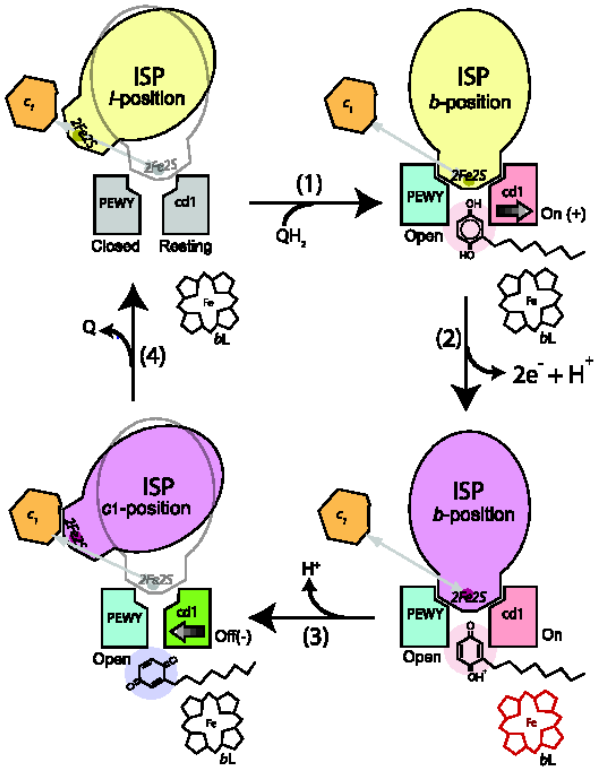

Figure 4. Control of the ISP-ED motion switch and the proposed mechanism for bifurcation of electron flow at the Q_P pocket

The structural components necessary for the control of the ISP conformational switch are illustrated in this cartoon rendition of the Q_P pocket. The PEWY motif and cd1 helix in gray represent a native (Resting) configuration. The ISPs in yellow and magenta are in oxidized and reduced forms, respectively. The heme b_L is red when it is reduced. The PEWY motif in blue stands for the open configuration as in the state with a bound Q_P site inhibitor. The cd1 helix in red symbolizes the conformation (On) as in the presence of a P_f inhibitor occupying the distal site (pink), and the cd1 helix in green shows the conformation (Off) when a P_m inhibitor is occupying the proximal site (purple). Cyt c_1 is shown in orange.

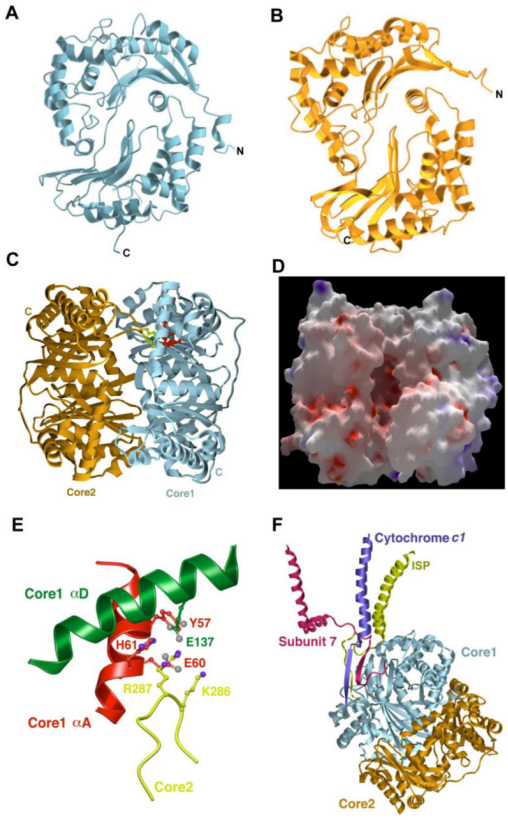

Figure 5. Structures of core proteins of bovine mitochondrial bc_1 complex

(A) Ribbon representation of the structure of the core-1 subunit showing two domains of the α-β structure related by an intradomain approximate twofold rotational axis perpendicular to the plane of the diagram (B) Structure of the core-2 in the form of a ribbon diagram showing in similar orientation as the core-1 subunit in (A). (C) Structure of core-1 (cyan) and core-2 (coral) heterodimer viewed parallel to the intersubunit approximate two-fold rotational axis. The two molecules are associated such that the N-terminal domain of core-1 is facing the C-terminal domain of core-2. The putative zinc-binding motif is shown as ball-and-stick models, which is detailed in (E). (D) Electrostatic potential surface representation of the core-1 and core-2 heterodimer. The surface is shown in the same orientation as in (C). Red surface represents negative potential and blue positive. (E) Structural arrangement of the zinc-binding motif in the core subunits of the bc_1 complex. Residues from the two α helices, αA (green) and αD (red) that are separated by more than 50 residues, contribute to the zinc-binding motif. Residues important for Zn binding from these two helices come together in the 3-D structure and are joined by ^{Bt}R287 and ^{Bt}K286 from the core-2 subunit (yellow). (F) Attachment of core proteins to the bc_1 complex. Core subunits are anchored to the TM region of the complex by recruiting and incorporating peptides from subunit 7 (red) and cyt c_1 (blue) into a β-sheet in the core-1 subunit. The ISP subunit (yellow) provides additional interactions with the core-1 subunit.

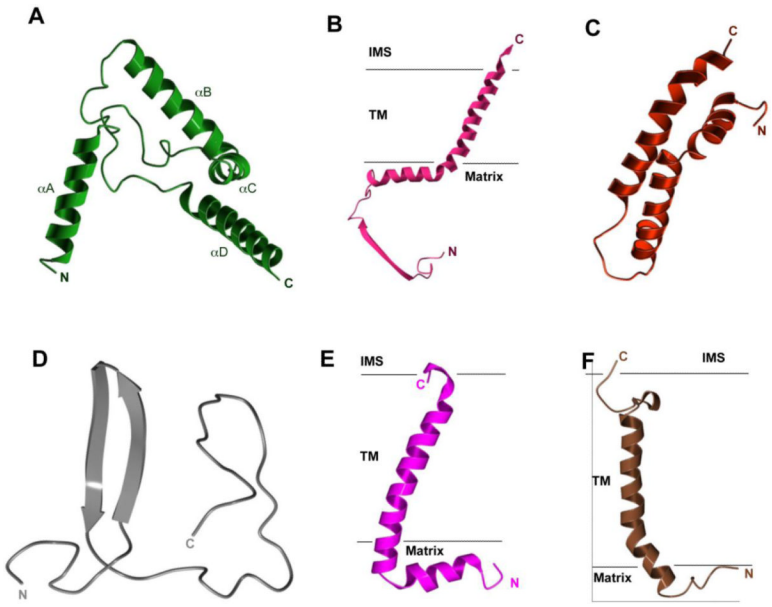

Figure 6. Structures of supernumerary subunits of the *Btbc*$_1$ complex in ribbon presentation
(A) Subunit 6, (B) subunit 7, (C) subunit 8, (D) subunit 9, (E) subunit 10, and (F) subunit 11.

Table 1

Available coordinates of deposited bc_1 structures or fragments determined by X-ray crystallography or EM

PDB ID	Orga[1]	Q_P site occupant[2]	Inhibitor Type	Q_N site occupant[3]	Reso[3] [Å]	R (free)[4]	No. subunits: *found/in vivo*	MW[5] (kDa)	SG	Ref
1RIE	B.T.	-	-	-	1.5		ISP-ED	14.6	$P2_1$	Iwata [16]
1SQB	B.T.	Azo	Pm	-	2.69	0.288	11 / 11	486	$I4_122$	Xia [58]
3L71	G.G.	Azo	Pm	Q10	2.84	0.281	10 / 11	486	$p2_12_12_1$	Berry TBP[6]
3L70	G.G.	Trifloxy	Pm	Q10	2.75	0.297	10 / 11	486	$p2_12_12_1$	Berry TBP
1SQP	B.T.	Myx	Pm	-	2.7	0.314	11 / 11	486	$I4_122$	Xia [58]
1SQQ	B.T.	MOAS	Pm	Q2	3.0	0.295	11 / 11	486	$I4_122$	Xia [58]
3L72	G.G.	Kres	Pm	Q10	3.06	0.294	10 / 11	486	$p2_12_12_1$	Berry TBP
3H1K	G.G.	Kres	Pm	Q10	3.48	0.284	10 / 11	486	$p2_12_12_1$	Berry [108]
3L73	G.G.	Triaz	Pm	Q10	3.04	0.293	10 / 11	486	$p2_12_12_1$	Berry TBP
1L0L	B.T.	Fam	Pf	-	2.35	0.306	11 / 11	486	$I4_122$	Xia [109]
3L74	G.G.	Fam	Pf	Q10	2.76	0.286	10 / 11	486	$p2_12_12_1$	Berry TBP
2FYU	B.T.	JG144	Pf	-	2.26	0.283	11 / 11	486	$I4_122$	Xia [57]
3L75	G.G.	Fen	Pf	Q10	2.79	0.275	10 / 11	486	$p2_12_12_1$	Berry TBP
3H1L	G.G.	Asc	Pf, PN	Asc	3.21	0.295	10 / 11	486	$p2_12_12_1$	Berry [110]
3CWB	G.G.	Croc	Pf	Q10	3.51	0.319	10 / 11	486	$p2_12_12_1$	Berry [111]
1NU1	B.T.	NQNO	Pf, PN	NQNO	3.2	0.296	11 / 11	486	$I4_122$	Xia [109]
1SQV	B.T.	UHDBT	Pf	Q2	2.85	0.285	11 / 11	486	$I4_122$	Xia [58]
1P84	S.C.	HDBT	Pf	Q6	2.5	0.252		467	$C2$	Hunte [24]
1SQX	B.T.	Stg	Pf	Q2	2.6	0.281	11 / 11	486	$I4_122$	Xia [58]
2A06	B.T.	Stg	Pf	Q10	2.1	0.258	10 / 11	486	$p2_12_12_1$	Berry [112]
1PP9	B.T.	Stg	Pf	Q10	2.1	0.287	10 / 11	486	$p2_12_12_1$	Berry [112]
1PPJ	B.T.	Stg	Pf	Ant	2.1	0.26	10 / 11	486	$p2_12_12_1$	Berry [112]
2BCC	G.G.	Stg	Pf	Q10	3.5	0.317	10 / 11	486	$p2_12_12_1$	Berry [112]
3BCC	G.G.	Stg	Pf	Ant	3.7	0.321	10 / 11	486	$p2_12_12_1$	Berry [18]
3H1I	G.G.	Stg	Pf	Ant	3.53	0.306	10 / 11	486	$p2_12_12_1$	Berry [110]

PDB ID	Orga[1]	Q_P site occupant[2]	Inhibitor Type	Q_N site occupant[3]	Reso[3] [Å]	R (free)[4]	No. subunits: *found/in vivo*	MW[5] (kDa)	SG	Ref
3H1J	G.G.	Stg	Pf	Q10	3.0	0.277	10 / 11	486	$p2_12_12_1$	Berry [18]
1EZV	S.C.	Stg	Pf	Q6	2.3	0.254	9 / 10	467	$C2$	Hunte [19]
1KB9	S.C.	Stg	Pf	Q6	2.3	0.249	9 / 10	467	$C2$	Hunte [91]
1KYO[7]	S.C.	Stg	Pf	-	2.97	0.268	9 / 10	467	$C2$	Hunte [87]
3CX5	S.C.	Stg	Pf	-	1.9	0.263	9 / 10	467	$C2$	Hunte [88]
2IBZ	S.C.	Stg	Pf	Q6	2.3	0.256	9 / 10	467	$C2$	Hunte [113]
3CXH	S.C.	Stg	Pf	-	2.5	0.256	9 / 10	467	$C2$	Hunte [88]
1ZRT	R.C.	Stg	Pf	-	3.5	0.358	3 / 3	221	$p2_1$	Berry [20]
2FYN	R.S.	Stg	Pf	-	3.2	0.254	3 / 4	250	$I4_122$	Xia [57]
2QJP	R.S.	Stg	Pf	Ant	2.6	0.277	3 / 4	250	$I4_122$	Xia [21]
2QJK	R.S.	Stg	Pf	Ant	3.1	0.266	3 / 4	250	$I4_122$	Xia [21]
2QJY	R.S.	Stg	Pf	Q2	2.4	0.251	3 / 4	250	$I4_122$	Xia [21]
2YIU	P.C.	Stg	Pf	-	2.7	0.29	3 / 3	467	$P2_1$	Hunte [22]
2YBB	T. T.	Stg	Pf	Q1	19.0	N/A	-	1,700		Kiirlbrandt [114]
1QCR	B.T.	-	-	-	2.7	0.375	11 / 11	486	$I4_122$	Xia [12]
1BE3	B.T.	-	-	-	3.0	0.32	11 / 11	486	$P6_522$	Iwata [17]
1BGY	B.T.	-	-	-	3.0	0.36	11 / 11	486	$P6_5$	Iwata [17]
1L0N	B.T.	-	-	-	2.6	0.297	11 / 11	486	$I4_122$	Xia [26]
1NTM	B.T.	-	-	-	2.4	0.285	11 / 11	486	$I4_122$	Xia [27]
1NTZ	B.T.	Q2	-	Q2	2.6	0.283	11 / 11	486	$I4_122$	Xia [27]
1NTK	B.T.	-	-	Ant	2.6	0.27	11 / 11	486	$I4_122$	Xia [27]
1BCC	G.G.	-	-	Q10	3.16	0.31	10 / 11	486	$p2_12_12_1$	Berry [18]
3H1H	G.G.	-	-	Q10	3.16	0.291	10 / 11	486	$p2_12_12_1$	Berry [18]

[1] Orga - organisms: B.T. , *B. taurus;* G.G., *G. gallus;* M.L., *M. laminosus;* NOS, *Nostoc sp. PCC7120;* T.H., *T. thermophilus;* C.R., *C. reinhardtii;* P.D.; *P. denitrificans;* R.S., *R. sphaeroides;* R.C., *R. capsulatus;* S.C., *S. cerevisiae*

[2] Q_P and Q_N site occupants: Azo, azoxystrobin; Trifloxy, trifloxystrobin; Myx myxothiazol; MOAS, MOA Stilbene; Kres, iodo-Kresoxim-dimethyl; Triaz, triazolone; Fam, famoxadone; Fen, fenamidone; Asc, ascochlorin; Croc, iodo-Crocacin-D; Stg, stigmatellin; Q2, ubiquinone Q2;Q10, ubuquinone Q10; Q6, ubiquinone Q6; Ant, antimycin.

[3] Reso: resolution or diffraction limit of the crystal in units of Å: 1Å = 10^{-10} m.

[4] Quality index; predictive power of model. A lower value of R (free) is better

[5] MW: Molecular weight of dimeric bc_1 complexes.

[6] TBP, to be published.

[7] in complex with cyt *c*.

Table 2

Edge-to-edge distances (Å, upper triangle) and calculated ET rates (s^{-1}, lower triangle) between pairs of prosthetic groups in dimeric bc_1 of space group $I4_122$ with the ISP in *b*-position

	$b_H(1)$	$b_L(1)$	$c_1(1)$	ISP(1)	$b_H(2)$	$b_L(2)$	$c_1(2)$	ISP(2)
$b_H(1)$	-	**7.9**	41.9	29.1	26.9	21.2	56.5	48.1
$b_L(1)$	$\mathbf{1.1\times10^{8}}$	-	27.5	22.4	21.2	**8.9**	40.4	34.2
$c_1(1)$	2.0×10^{-13}	5.3×10^{-4}	-	**27.7**	56.5	40.4	49.5	54.7
ISP(1)	1.6×10^{-5}	0.85	$\mathbf{2.1\times10^{-5}}$	-	48.1	34.2	54.7	59.8
$b_H(2)$	4.9×10^{-5}	0.83	2.4×10^{-22}	4.2×10^{-17}	-	7.9	41.9	29.1
$b_L(2)$	0.83	$\mathbf{4.7\times10^{6}}$	7.2×10^{-12}	5.4×10^{-8}	$\mathbf{1.1\times10^{8}}$	-	27.5	22.4
$C_1(2)$	2.4×10^{-22}	7.2×10^{-12}	8.0×10^{-19}	7.2×10^{-22}	2.0×10^{-13}	5.3×10^{-4}	-	27.7
ISP(2)	4.2×10^{-17}	5.4×10^{-8}	7.2×10^{-22}	4.2×10^{-25}	1.6×10^{-5}	0.85	2.1×10^{-5}	-

The calculated ET rates (k_{et}, s^{-1}), using the empirical expression $\log k_{et} = 15.2 - 0.61R - 3.1\,(\Delta G-\lambda)^2/\lambda$ for weakly coupled donor-acceptor pairs [31], are based on edge-to-edge distances of R in Å, a driving force (ΔG°) under standard conditions of −0.13 eV for the donor-acceptor pairs of b_L-b_H and b_H-c_1, of −0.15 eV for the b_H-ISP pair, of 0 eV for the pairs of b_H-b_H, b_L-b_L, c_1-c_1, and ISP-ISP, of −0.26 eV for the b_L-c_1 pair, and −0.28 eV for the b_L-ISP pair, and a reorganization energy (λ) of 1.0 eV recommended for protein media.

Table 3

Conformational switch of the ISP-ED for the iron atoms of the ISC in different crystal forms and with different bound inhibitors

Space group	Organism	Ligand at Q_P site	ISP position	Normalized ISC ano peak[a]	ISC-heme c_1 distance (Å)	Estimated ET rate (s^{-1})	Ref.
$I4_122$	*B. t.*	None	*m*[c]	0.45	27.7	2.1×10^{-5}	Xia [32]
$I4_122$	*B. t.*	Azoxystrobin	*m*[c]	0.36	27.7	2.1×10^{-5}	Xia [57]
$I4_122$	*B. t.*	MOAS	*m*[c]	0.23	27.7	2.1×10^{-5}	Xia [57]
$I4_122$	*B. t.*	Famoxadone	*b*[d]	1.02	27.7	2.1×10^{-5}	Xia [57]
$I4_122$	*B. t.*	Stigmatellin	*b*[d]	1.20	27.7	2.1×10^{-5}	Xia [57]
$I4_122$	*B. t.*	UHDBT	*b*[d]	0.96	27.7	2.1×10^{-5}	Xia [57]
$P6_5$	*B. t.*	None	*n1*[e]	-	23.6	0.007	Iwata [17]
$P6_522$	*B. t.*	None	c_1[f]	-	7.8[b]	2.9×10^{7}	Iwata [17]
$P2_12_12_1$	*B. t.*	Kresoxim-dimethyl	*n2*	-	14.9[b]	1361	Berry[TBP]
$P2_12_12_1$	*B. t.*	Stigmatellin	*b*	-	27.7	2.1×10^{-5}	Berry [112]
$C2$	S. c.	Stigmatellin	*b*	-	26.8	7.5×10^{-5}	Hunte [19]
$P2_12_12_1$	*B. t.*	Azoxystrobin	*n2*[f]	-	14.6[b]	2074	Berry[TBP]
$C2$	*R. s.*	Stigmatellin	*b*	-	27.0	5.7×10^{-5}	Xia [21]
$P2_1$	*R. s.*	Stigmatellin	*b*	-	27.0	5.7×10^{-5}	Xia [21]

TBP. To be published

[a] Normalized anomalous difference Fourier peaks for the Fe atoms in the ISP subunits [58]

[b] Distances are measured from ND2 of H161 of ISP to closest atom on the ring of heme c_1

[c] ISC at *b*-position is of low occupancy

[d] ISC at *b*-position is of high occupancy

[e] ISC at intermediate-1 position

[f] ISC at c_1-position

[g] ISC at intermediate-2 position